sPHENIX Simulation Note

sPH-HF-2017-002

D^0-meson and B^+-meson production in Au+Au Collisions at $\sqrt{s_{\mathrm{NN}}}$ = 200 GeV for sPHENIX

Xiaolong Chen (xlchenustc@gmail.com),[1,2] Xin Dong (xdong@lbl.gov),[2] and Guannan Xie (xgn1992@mail.ustc.edu.cn)[1,2]

[1] *University of Science & Technology of China, Hefei 230026, China*

[2] *Lawrence Berkeley National Laboratory, Berkeley, California 94720, USA*

(Dated: July 9, 2017)

Contents

1. GOAL

Heavy flavor quarks (c, b), due to their large masses, are expected to have unique roles for studying QCD in both vacuum and medium. There have been extensive measurements of heavy quark production in elementary collisions that demonstrate their production is calculable in perturbative QCD. Heavy quark interaction with hot Quark-Gluon Plasma (QGP) should shed light on the roles of radiative energy loss vs. elastic collisional energy loss in such a medium. In particular, one should expect the mass hierarchy for the parton energy loss in QCD medium: $\Delta E_b < \Delta E_c < \Delta E_q < \Delta E_g$. The heavy quark propagation inside the QGP medium can be treated as "Brownian" motion when the heavy quark mass is much larger than the medium temperature as well as the interaction strength. The heavy quark equation of motion can be described by a reliable stochastic Langevin simulation and characterized by one intrinsic medium transport parameter - the heavy quark diffusion coefficient. Here low p_{T} measurements will be more relevant for the determination of this transport parameter.

There have been great achievements in heavy flavor measurements in the past few years with new instrumentation and large datasets collected at RHIC and LHC. At the QM17 conference, we have seen clear evidences that charm quarks flow the same as other light hadrons and strong suppression in R_{AA}, which indicates charm quarks may be thermalized in the QGP medium at top RHIC and LHC energies. We also see evidences of less energy loss for bottom quarks than charm or light quarks, consistent with the suppression mass hierarchy of parton energy loss.

The next phase of heavy quark program will be focusing on precision open bottom measurements and heavy quark correlations. We have observed the evidences of mass hierarchy of parton energy loss. A detailed investigation on open bottom production in heavy-ion collisions will be necessary to evaluate quantitatively the roles between radiative energy loss vs. collisional energy loss. Open bottom production will also offer the cleanest way to measure the heavy quark diffusion coefficient due its much larger quark mass compared to the charm quark. Total bottom yield will further help a precision interpretation of Upsilon results measured in heavy-ion collisions. This requires precision measurements down to low or even zero p_{T}.

The goal of this analysis is to estimate the performance of measuring D^0-meson and B-meson production in Au+Au collisions at $\sqrt{s_{\mathrm{NN}}}$ = 200 GeV for sPHENIX with the Monolithic Active Pixel Sensor Vertex Detector (MVTX) [1]. The estimation for D^0-mesons includes both prompt D^0 and non-prompt D^0 which are from B-decay.

Through non-prompt D^0 production and direct B^+ measurement, we can measure the total $b\bar{b}$ cross-section at midrapidity ($d\sigma_{b\bar{b}}/dy$) in Au+Au collisions at $\sqrt{s_{_{\rm NN}}}$ = 200 GeV. Systematic investigations of charm and bottom hadron production in heavy-ion collisions will shed light on parton energy loss in the Quark-Gluon Plasma (QGP), which can help constrain the transport parameters of the QGP medium. By measuring prompt D^0 and non-prompt D^0 v_2 we can study charm and bottom flow and the interaction between heavy quarks and the QGP medium.

2. SIMULATION APPROACH

The simulation approach in this analysis is a hybrid fast Monte Carlo (MC) method with full GEANT + tracking input. With this method, one can obtain sufficient MC statistics for uncertainty estimation of physics observables without running millions of full GEANT + tracking simulations which are very time intensive (CPU time ratio between full GEANT+tracking simulation and fast MC is $\sim 10^6$ for central collisions). We will also show in this section the hybrid fast MC method can reproduce both the signal efficiency and background acceptance rate with reasonable precision. The key ingredients are:

- run the full GEANT + tracking simulation with embedded single particles to gain statistics over a wide momentum region.
- the detector response is characterized by single track performance distributions: TPC tracking efficiency, MAPS matching efficiency, DCA_{XY} vs DCA_Z 2D distributions, momentum resolution, etc.
- For signals, we run the $D^0 \to K^-\pi^+$ decays or $B+$ meson decays with PYTHIA decayers. The decay distance distributions follow the particle lifetime with Lorentz boost. For background, we sample the stable particle π, K and p distributions according to the HIJING event generator output.
- then for all final stable particles, we smear their position and momentum distributions according to the DCA and momentum resolution obtained from full simulation above. The tracking and MVTX matching efficiency will be also applied here.
- then follow the real data analysis to do topological reconstruction, apply topological cuts and estimate the final accepted signal and background counts that will be used to estimate the signal significance in each p_T bin.

2-1. sPHENIX Detector Performance

sPHENIX detector performance was studied by running sPHENIX full GEANT simulation with 100 $K/\pi/p$ embedded in central HIJING events with impact parameter less than 4.4 fm.

The simulation was carried out using the simulation and tracking software as of Jan. 2017. The new tracking software is under development and a tagged version at this stage is not ready yet. The simulation and tracking were done with 3 layers of MVTX, 4 layers of INTT and 60 layers of TPC with their locations positioned in the nominal radii according to the MVTX, INTT designs. The TPC simulation includes the effect of space charge distortion to the level as described in Tony's presentation in the tracking review in Sept. 2016.

Fig. 1 is $K/\pi/p$ tracking efficiency as a function of p_T, which includes TPC tracking efficiency and at least two layers MAPS hits. We parametrized the distributions with the function shown in Eq. 1.

$$Eff = N \times e^{-(p_T/a)^b} \tag{1}$$

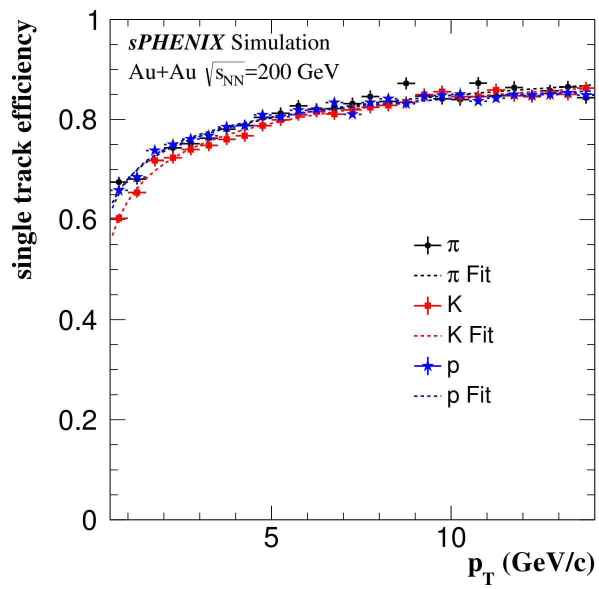

FIG. 1: $K/\pi/p$ tracking efficiency from full GEANT + tracking simulation with single particles embedding in central Hijing events in Au+Au collisions at $\sqrt{s_{NN}}$ = 200 GeV

Fig. 2 left panel shows a Gaussian fit for $K/\pi/p$ momentum resolution at $2.0 < p_T < 2.2$ GeV/c; and then right panel shows the $K/\pi/p$ momentum resolution as a function of p_T. Eq. 2 is the fitting function.

$$\frac{\sigma_{p_T}}{p_T} = \sqrt{(\frac{a}{\sqrt{p_T}})^2 + (b \cdot p_T)^2 + c^2} \tag{2}$$

Fig. 3 left panel shows the $K/\pi/p$ DCA_{XY} distributions at $2.0 < p_T < 2.5$ GeV/c and the Gaussian fit to them. The right panel shows the $K/\pi/p$ DCA_{XY} resolutions (obtained through the

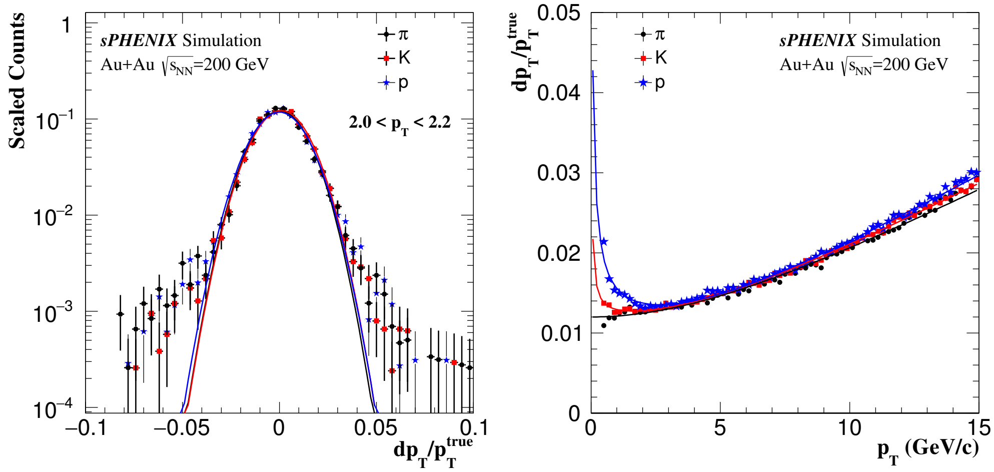

FIG. 2: (Left) dp_T/p_T^{true} distributions for $K/\pi/p$ particles in the p_T region of 2.0-2.2 GeV/c and fitted with Gaussian functions. (Right) Momentum resolution (width from Gaussian fits) as a function of p_T.

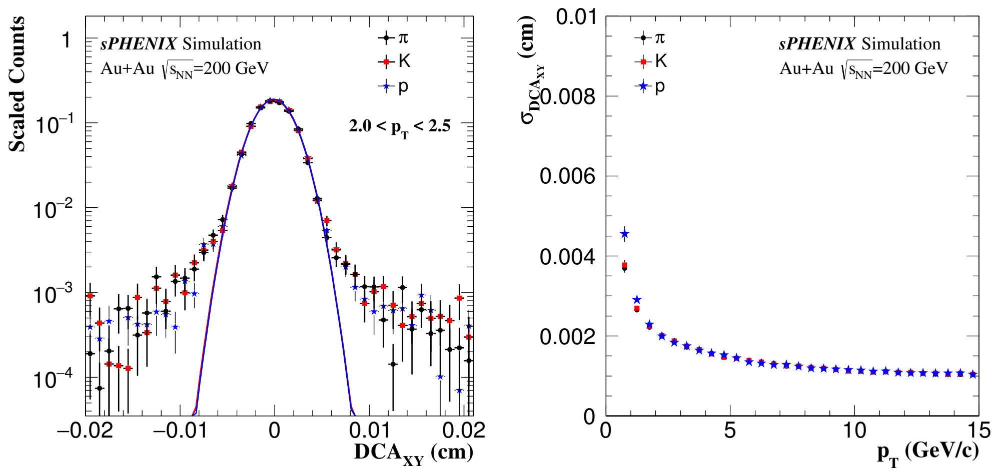

FIG. 3: (Left) DCA_{XY} distributions for $K/\pi/p$ particles in the p_T region of 2.0-2.5 GeV/c and fitted with Gaussian functions. (Right) DCA_{XY} resolution (width from Gaussian fits) as a function of p_T.

Gaussian fits) as a function of p_T. DCA is Distance of Closest Approach between particle track and primary vertex. The same exercise was done for DCA_Z, shown in Fig. 4.

In the barrel-like detector configuration (TPC, MVTX etc.), one has to consider the correlation between DCA_{XY} and DCA_Z. With the STAR HFT experience, it was demonstrated that if one only samples the DCA_{XY} and DCA_Z distributions independently, one cannot reproduce the 3D DCA distributions seen in data. When considering the DCA_{XY} vs DCA_Z 2D correlation, the 3D DCA distributions are nicely reproduced. Fig. 5 is an example of pion DCA_{XY} vs DCA_Z 2D

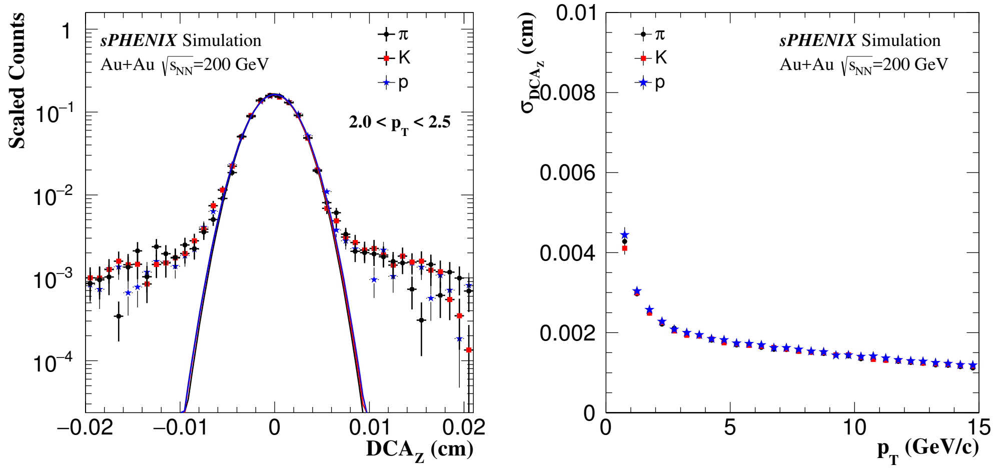

FIG. 4: (Left) DCA_Z distributions for $K/\pi/p$ particles in the p_T region of 2.0-2.5 GeV/c and fitted with Gaussian functions. (Right) DCA_Z resolution (width from Gaussian fits) as a function of p_T.

distribution at $0.4 < p_T < 0.5$ GeV/c.

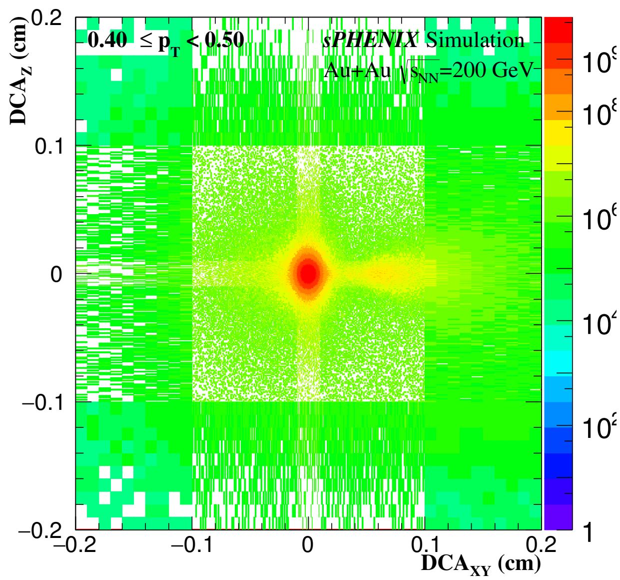

FIG. 5: π DCA_{XY} vs. DCA_Z 2D distribution in the region of 0.4$<$ p_T $<$ 0.5 GeV/c.

2-2. Fast Simulation Package

After all the input ingredients from full GEANT simulation are ready, the fast simulation basic recipe is:

- Sample primary collision vertex (v_x, v_y, v_z) distributions. At this moment all primary vertex positions are fixed to (0,0,0). We didn't consider the primary vertex resolution which can be ignored in AuAu central collisions.

- Throw signal (D^0, B) or background ($K/\pi/p$ from HIJING) tracks into the Fast Simulation Package. For the signal we sample a distribution flat in p_T, rapidity(y), ϕ and let it decay. Use p_T shape from real data or FONLL or other models as weight. The total signal number per event will be controlled with measured (or theory calculated) cross sections. For background, we consider both primary and secondary $K/\pi/p$ tracks in the Fast Simulation Package, $K/\pi/p$ original MC position is fixed to 0, and with flat η, ϕ. p_T shape is from published paper (Fig. 6). And $K/\pi/p$ number per event is taken from HIJING using the total number of particles seen in the same kinematic and DCA range, see Fig. 7.

- Smear $K/\pi/p$ momentum according to the momentum resolution.

- Smear $K/\pi/p$ track origin position with DCA_{XY} vs DCA_Z 2D distribution.

- Apply tracking efficiency, TOF matching efficiency (if needed) to the smeared $K/\pi/p$ tracks.

  The Time-Of-Flight (TOF) particle identification detector is not in the sPHENIX baseline detector. There is a 10-cm physical gap between the out field cage of TPC and the EMCal detector which may be potentially used for a TOF detector. The default sPHENIX configuration will be no PID case, while we also include certain PID capability enabled by a possible future TOF detector in our simulation. The TOF PID capability is assumed to be the same the STAR TOF detector which requires 25ps timing resolution. We considered the following three cases:

  1. **no PID** case: all particles are mis-identified. There will be lots of background.
  2. **hybrid PID** case: at $p_T < 1.6$ GeV/c, use TOF while TOF is avaliable, otherwise apply no PID. At $p_T > 1.6$ GeV/c, apply no PID. TOF matching efficiency is defined by track number with TOF match over total TPC track number. Assume TOF matching efficiency is $f(p_T)$ and TOF PID efficiency is 100%, if $gRandom \rightarrow Rndm() > f(p_T)$, it means without TOF match, particle will be mis-identified. In this simulation, we use two kinds of TOF matching efficiency. One is assuming ideal TOF with 100%

matching and the other is applying TOF matching efficiency from STAR Run14 data (Fig. 8).

3. **clean PID** case: at $p_T < 1.6$ GeV/c, must use TOF. This will lose efficiency, but may much decrease background. At $p_T > 1.6$ GeV/c, apply no PID. In this PID case, at $p_T < 1.6$ GeV/c, particle will not be mis-identified.

- Reconstruct topological structure: Use $D^0 \to K^-\pi^+$ as an example. With smeared K/π position and momentum, the reconstructed K/π tracks are formed. We can obtain K/π DCA (to primary vertex) directly. Then calculate the closest points between two reconstructed K/π tracks. The distance between the two closest points is $dcaDaughters$ and the their average position is D^0 decay vertex (secondary vertex). Distance between secondary vertex and primary vertex is decay length. With reconstructed D^0 momentum and its decay vertex, we can calculate D^0 DCA (to primary vertex) and $\cos\theta$, where θ is the angle between D^0 momentum direction and the direction from primary vertex pointing to secondary vertex.

- Apply topological cuts to obtain reconstructed signal and background counts in any given number of events.

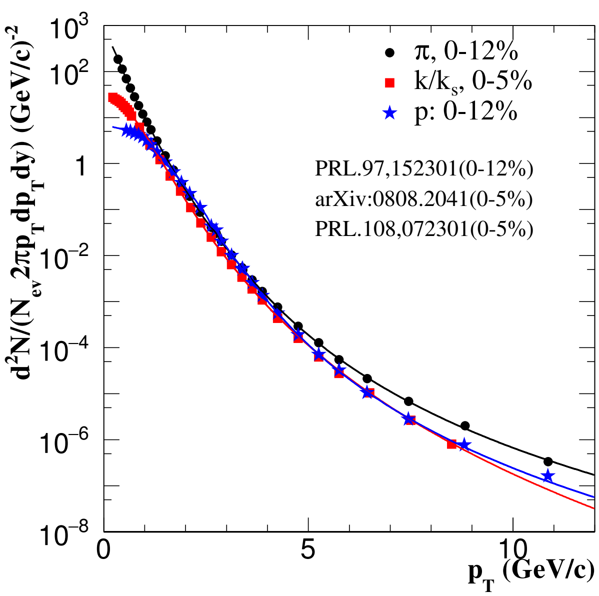

FIG. 6: $\pi/K/p$ spectra in AuAu 200 GeV from previous publications[2–4]

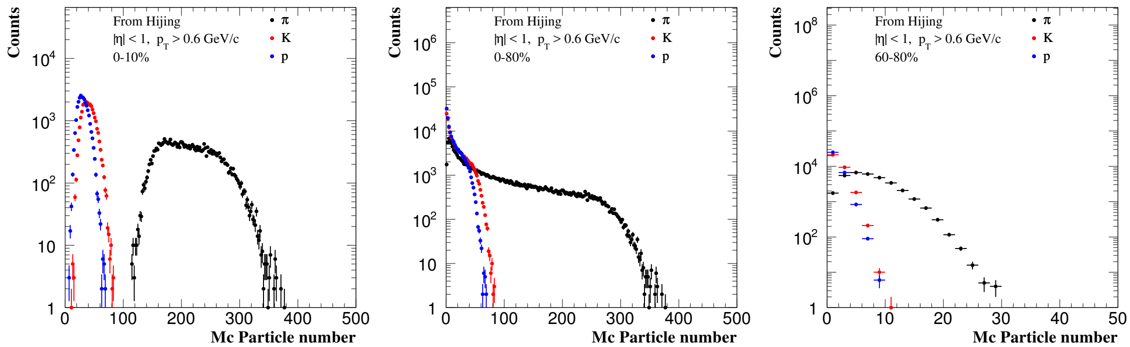

FIG. 7: $\pi/K/p$ number from HIJING in 0-10%, 0-80%, and 60-80% Au+Au collisions.

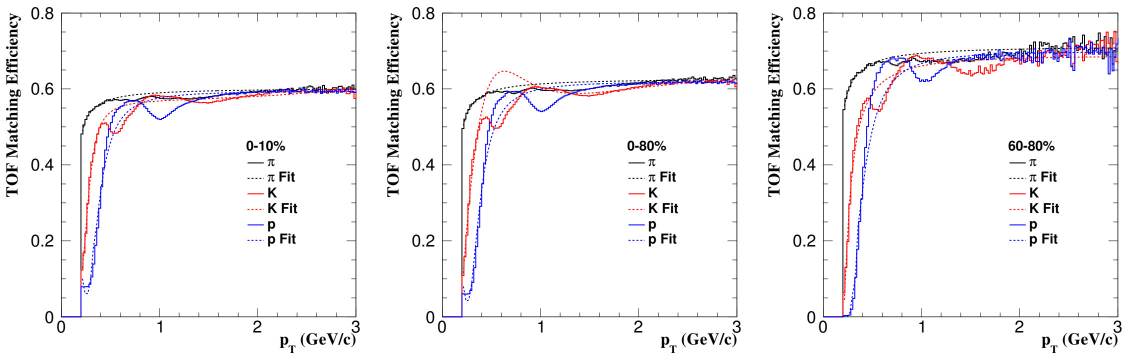

FIG. 8: $\pi/K/p$ TOF matching efficiency from STAR Run14 in 0-10%, 0-80%, and 60-80% Au+Au collisions.

2-2-1. Validation of signal simulation

This fast MC simulation method has been validated with full GEANT + tracking simulation. For signals, we tested it with D^0 embedded in central HIJING (0-10%). Fig. 9 is the validation procedure and workflow. By running D^0 embedded HIJING production, we can get D^0 efficiency and some topological value (for example K/π DCA, D^0 DCA, DCA between $K\pi$, $\cos\theta$, decayLength) distributions directly from the production. We can also get TPC track efficiency, MAPS match ratio, momentum resolution, etc. from HIJING production, and input these to our Fast Simulation Package. And then we can also get D^0 efficiency, topological value distributions by running Fast Simulation Package. We then can compare the results from the two methods to see whether Fast Simulation Package reproduces the signal efficiency as well as various topological variable distributions.

Fig. 10 left panel shows the efficiency comparison between pure HIJING (true efficiency) and

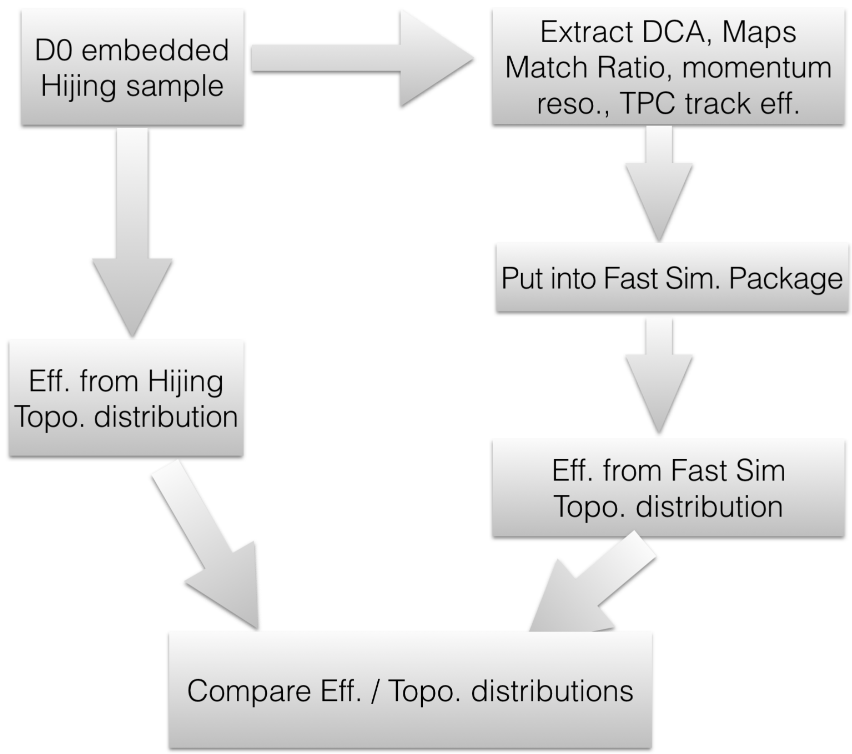

FIG. 9: Signal validation procedure and workflow with HIJING + D^0 embedding

Fast Simulation (validated efficiency) and the ratio between the two is shown on the right panel. They are consistent with each other within 5% given the current statistics. The acceptance $\times$ efficiency is defined as the fraction of total MC D^0 within $|y| < 1$ that contain decay daughters with $p_T > p_T^{\mathrm{th}}$ GeV/c and $|\eta| < 1$, reconstructed with sPHENIX tracking, and the single/pair geometry parameters passing the topological cuts. We often factorize the acceptance as the fraction of total MC D^0 within $|y| < 1$ that contain decay daughters within the p_T and η window. The tracking efficiency and topological cut efficiency are added together as the D^0 efficiency.

Fig. 11 shows topological variable distribution comparisons between pure HIJING and Fast Simulation. The agreement between the two is very good for all five topological variables.

2-2-2. Validation of background simulation

Fig. 12 shows the procedure and workflow to validate background rates with the fast simulation package. It's very similar to the signal validation. From HIJING production, we can extract not only TPC track efficiency, MAPS match ratio, momentum resolution, but also K/π η, ϕ, p_T and numbers per event.

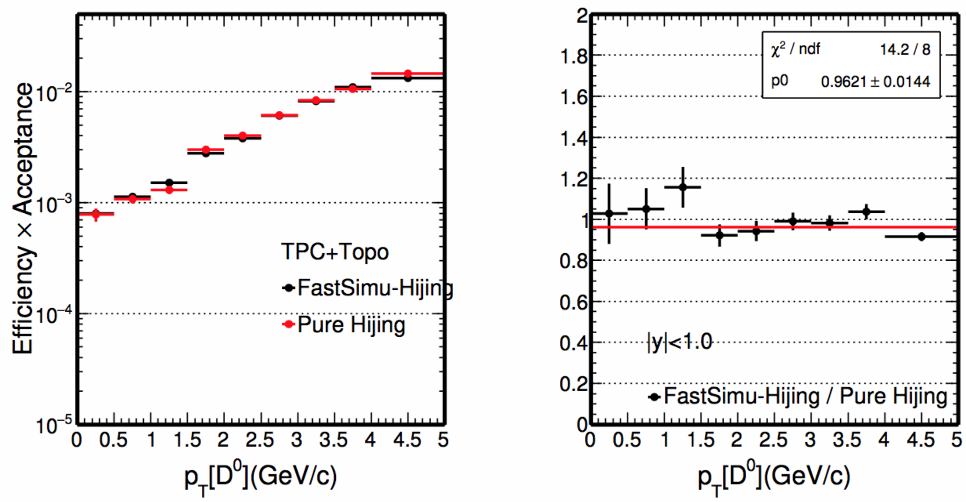

FIG. 10: D^0 efficiency comparison between HIJING and Fast Simulation in 0-10% central HIJING simulation with D^0 embedded in.

Fig. 13 shows the background $K\pi$ invariant mass distribution comparison in different p_T bins between HIJING and Fast Simulation. They are under the same cuts described in Fig. 10. It shows fast simulation package works well for background rate estimation.

Regarding signal and background topological reconstruction, please see Section 3-2 for details.

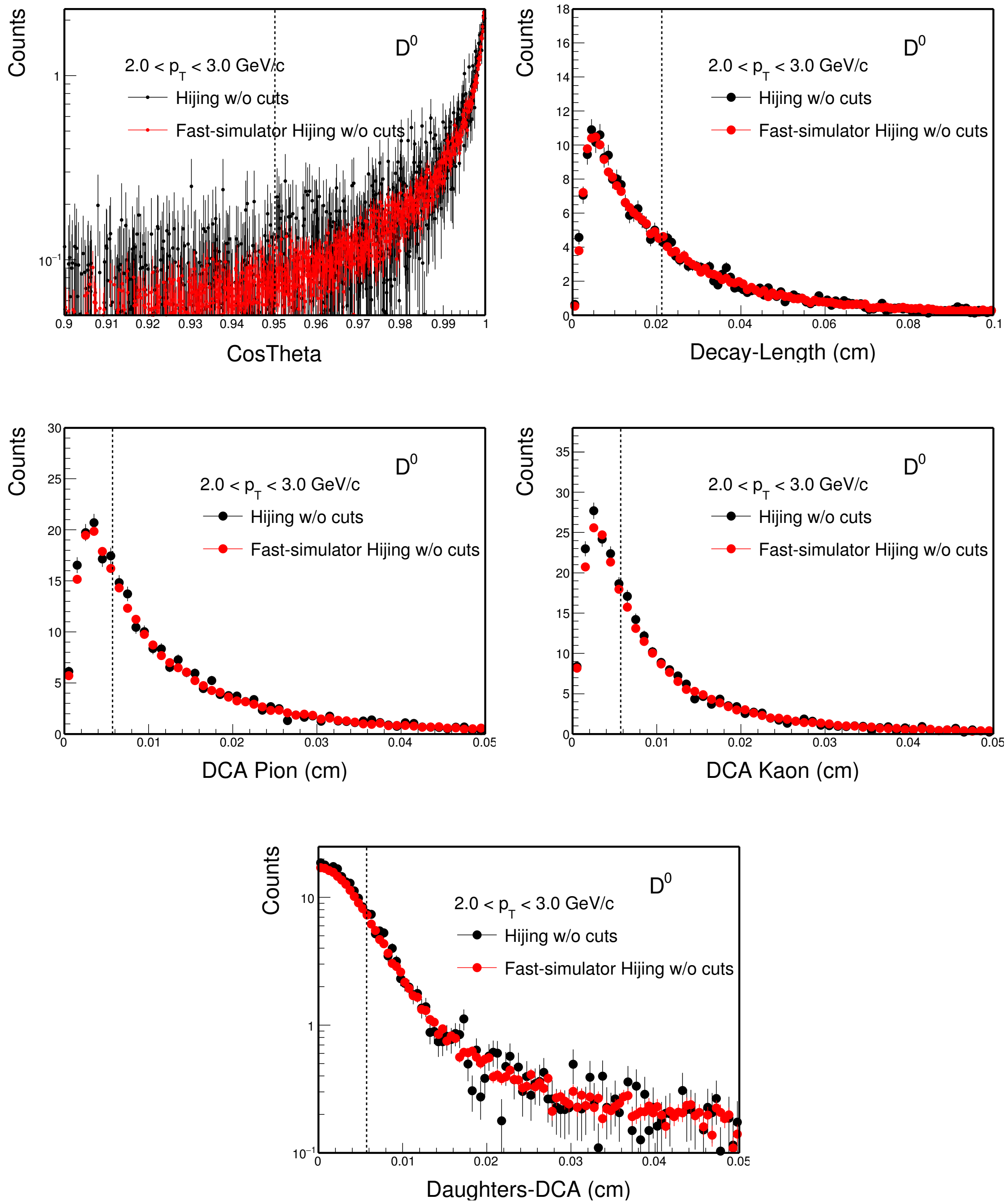

FIG. 11: D^0 topological variable comparison between HIJING and Fast Simulation in 0-10% central HIJING simulation with D^0 embedded in

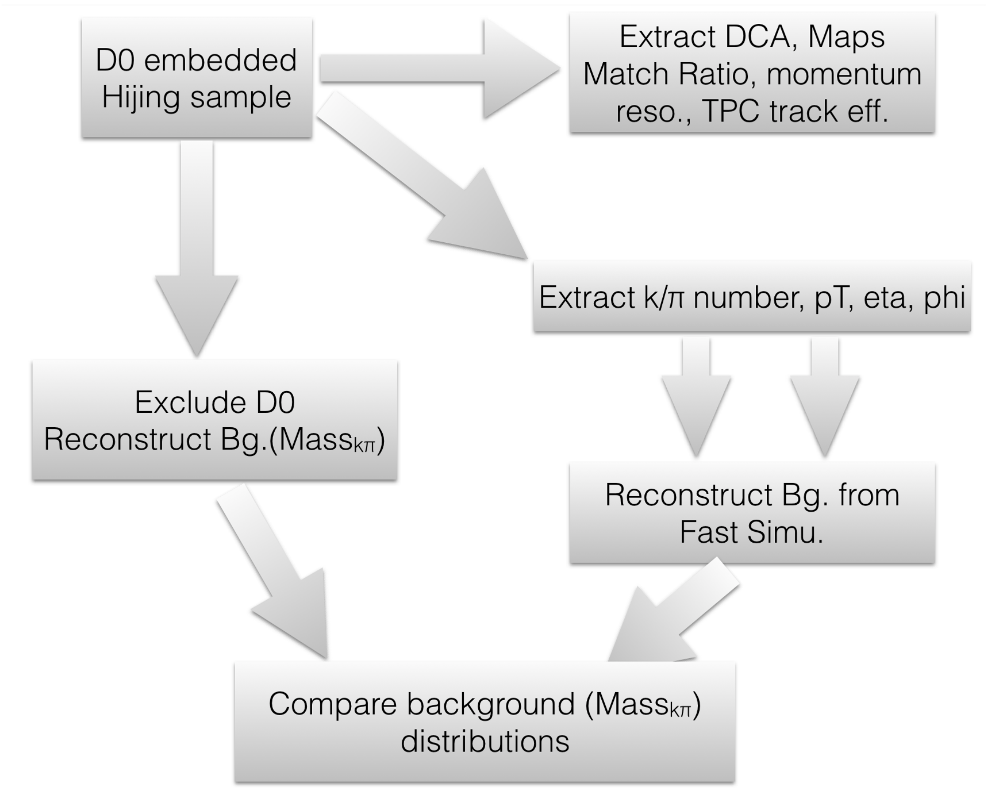

FIG. 12: Background validation procedure and workflow with HIJING production

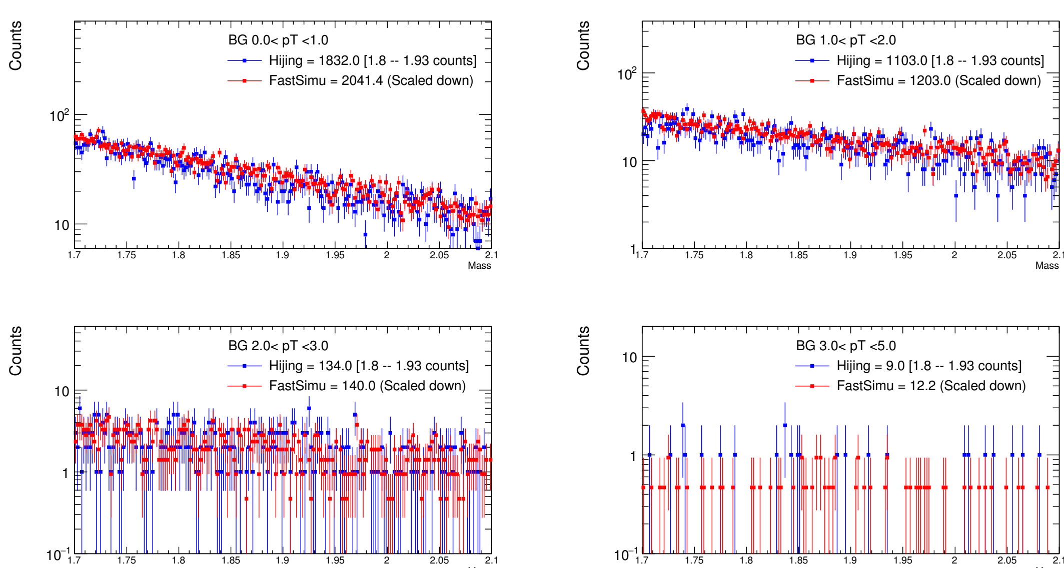

FIG. 13: Background $K\pi$ invariant mass distribution comparison between HIJING and Fast Simulation in 0-10% Au+Au collisions.

3. D^0 MEASUREMENT

3-1. Signal and combined background simulation

We followed the procedure described in Section. 2 2-2 for D^0 background and signal simulation.

Prompt D^0 particles are forced to decay to kaons and pions ($D^0 \to K^-\pi^+$) with 100% branch ratio (B.R. rescaled later). We sample flat in rapidity from -1 to 1, flat ϕ from 0 to 2π, and flat p_T from 0 to 20 GeV/c. And p_T weights will be applied later using the STAR Run14 data.

For the non-prompt D^0 signal, the input particles are $B^0(\bar{B}^0)$ and $B^\pm$. All channels in PYTHIA version 6.416 that decay to D^0 ($B \to D^0X$) are included. Relative contributions of B^+, B^0 to non-prompt D^0 are fixed using fragmentation and branching ratios listed in Table. I. We sample flat p_T from 0 to 20 GeV/c, flat ϕ from 0 to 2π, and flat rapidity from -1.5 to 1.5. We choose a wider rapidity window of $|y|$ <1.5 instead of 1 because non-prompt D^0 at $|y| < 1$ may come from B-meson at $|y| > 1$. We use the p_T shape from FONLL ($\times R_{AA}$) for the weight factors (Fig. 14). R_{AA} is an empirical average of three model calculations from CUJET 3.0, TAMU and Duke [5, 6]. We let B-mesons decay to D^0 first and then let the D^0 decay to kaon and pion.

D^0 and B-meson cross section values are also listed in Table. II.

Particle	$c\tau$ (μm)	Mass (GeV/c)	$q(c,b) \to X(FR)$	$X \to D^0(\bar{D}^0)(BR)$
D^0	123	1.865	0.565	-
B^0	459	5.279	0.40	0.081(0.474)
B^+	491	5.279	0.40	0.086(0.790)

TABLE I: D^0 and B-meson particle properties from the PDG.

	0-10%	0-80%	60-80%
D^0	AuAu data	AuAu data	pp data $\cdot$ N_{bin}
B	pp FONLL $\cdot$ R_{AA} $\cdot$ N_{bin}	pp FONLL $\cdot$ R_{AA} $\cdot$ N_{bin}	pp FONLL $\cdot$ N_{bin}

TABLE II: D^0 and B-meson cross section in different centralities

Combinatorial background are random combinations of π, K ($\to D^0$). Particle misidentification will increase the background. In this simulation, we consider the following three cases (Single

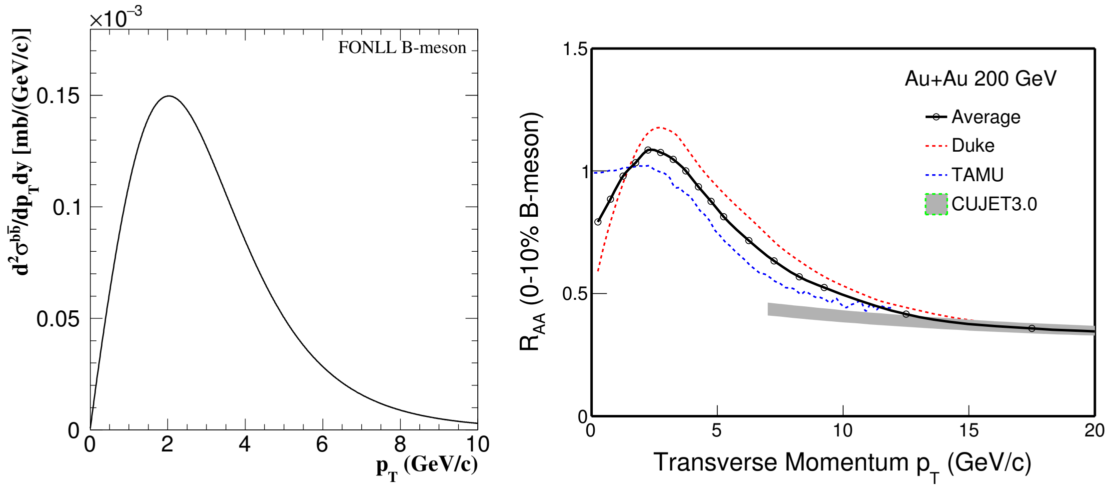

FIG. 14: B-meson p_T spectra from FONLL [7] and R_{AA} at 0-10% [5, 6]

particle PID is defined in Section. 2 2-2):

1. **w/o TOF** : no particle identification for all final state particles. So every track will be consider as both a kaon and a pion candidate when forming pairs. In this case, no additional signal efficiency loss due to (mis-)PID, but background levels will be higher due to mis-PID.

2. **with TOF** : assuming the same PID capability as STAR TOF which has a clean separation between Kaons/pions up to around 1.6 GeV/c. We also take the same TOF acceptance + matching + PID efficiency from STAR Run14 data. (Fig. 8). Since final state particles are pions dominated, we always apply strict PID for Kaon candidates when the TOF PID is capable (<1.6 GeV/c) while we only require TOF PID for pion candidates when TOF information is available. Due to the finite TOF acceptance, matching and PID efficiency, there will be some amount efficiency loss for signals.

3. **with ideal TOF** : Assuming TOF matching efficiency is 100%. We apply clean PID for both kaon sample and pion sample to ensure they are pure. Both signal and background won't have efficiency loss from TOF.

We have only run the full GEANT + tracking simulation for 0-10% Hijing events to obtain the detector response distributions. We apply the same detector response input to 0-80% and 60-80% centrality bins later to calculate projections for physics observables. We consider that these are conservative estimates since typically the tracking performance is the worst in the most central collisions with highest multiplicity/detector occupancy. (Section. 2 2-1).

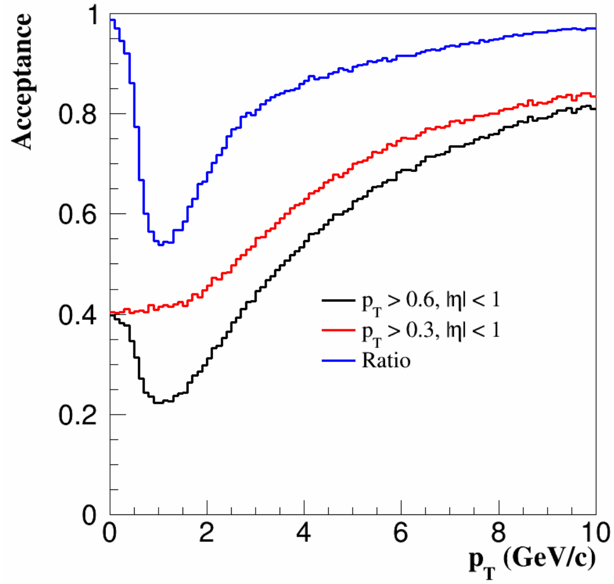

FIG. 15: D^0 acceptance as a function of p_T for two different daughter p_T cut and the ratio between the two.

3-2. Topological cuts tuning

The single track acceptance cuts applied in the following analysis are $p_T > 0.6$ GeV/c and $|\eta| < 1$ for both kaons and pions. The p_T cut threshold is a tunable parameter. We inherited the 0.6 GeV/c default cut from the STAR HFT analysis. The reason is to control the fake hit rate in the HFT detector. Lowering this p_T threshold cut can further improve the low p_T D^0 acceptance. Figure 15 shows the D^0 acceptance as a function of p_T for two different daughter p_T cut and the ratio between the two.

We consider 6 topological variables for prompt D^0, and 5 topological variables for non-prompt D^0 (no DCA_{D^0}) in our cut optimization study. The reason for excluding D^0 DCA cut for non-prompt D^0 is that in real data analysis, prompt D^0 and non-prompt D^0 are merged together and D^0 DCA distributions are used to separate them. Fig. 16 is a cartoon of prompt D^0 (left) and one case of non-prompt D^0 (right) decay structure. The topological variables are:

- π DCA: the Distance of Closest Approach from π track to PV (Primary Vertex).
- K DCA: the Distance of Closest Approach from K track to PV.
- $dcaDaughters$: closest distance between K and π.
- D^0 DCA: see the cartoon picture.

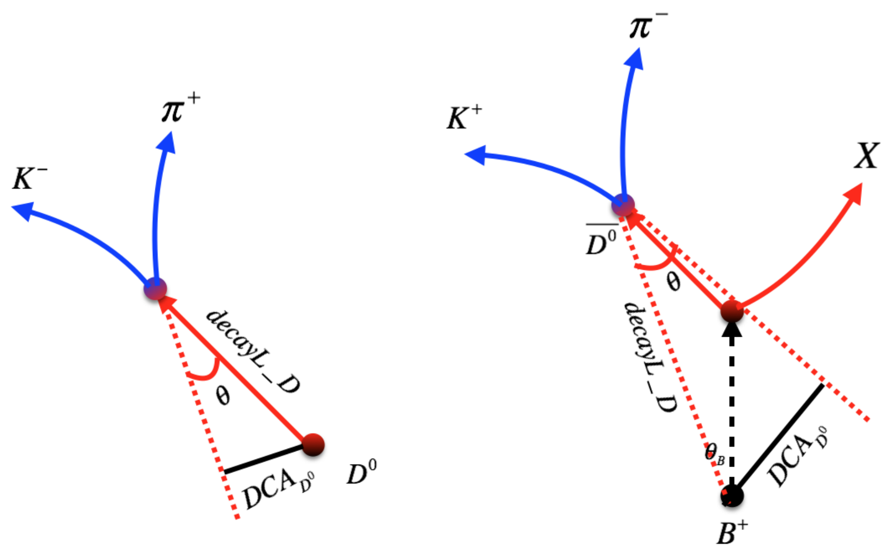

FIG. 16: Cartoon of prompt D^0 (left) and one case of non-prompt D^0 (right) decay structure

- $decayLength$: see the cartoon picture.
- $\cos\theta$: see the cartoon picture.

The cuts from these variables are tuned with the Toolkit for Multivariate Data Analysis (TMVA) package [8] in 7 D^0 p_T bins (0-1, 1-2, 2-3, 3-4, 4-5, 5-7, 7-10 GeV/c). "Cuts method" (rectangle cuts) in the TMVA package is selected. This option scans different rectangle cuts in the multi-variable space, calculates signal and background efficiency for each cut set, selects the cuts with lowest background efficiency at every signal efficiency bin (1% bin width).

We only tuned topological cuts for non-prompt D^0 at 0-10% and 60-80% for the no-PID case. For the reconstruction in 0-80% centrality, we use the same cuts as 0-10%, and also in the case of TOF PID we use the same cuts as noPID case. In the TMVA training, we ran 100 million events for background and 40 million B-mesons in 0-10% centrality, and 1 billion events for background and 40 million B-mesons in 60-80% centrality, respectively. The input tree for TMVA package is within 3σ mass window ($1.82 < m_{K\pi} < 1.91$ GeV/c^2) both for signal and background. The signal (non-prompt D^0) and background entries are both rescaled to 10 billion events for 0-10% and 60-80%.

In order to save CPU time, the background at low p_T (< 2 GeV/c) is randomly excluded, but add another weight to compensate the lost background.

Fig. 17 shows example distributions of 5 topological variables for non-prompt D^0 signal (blue)

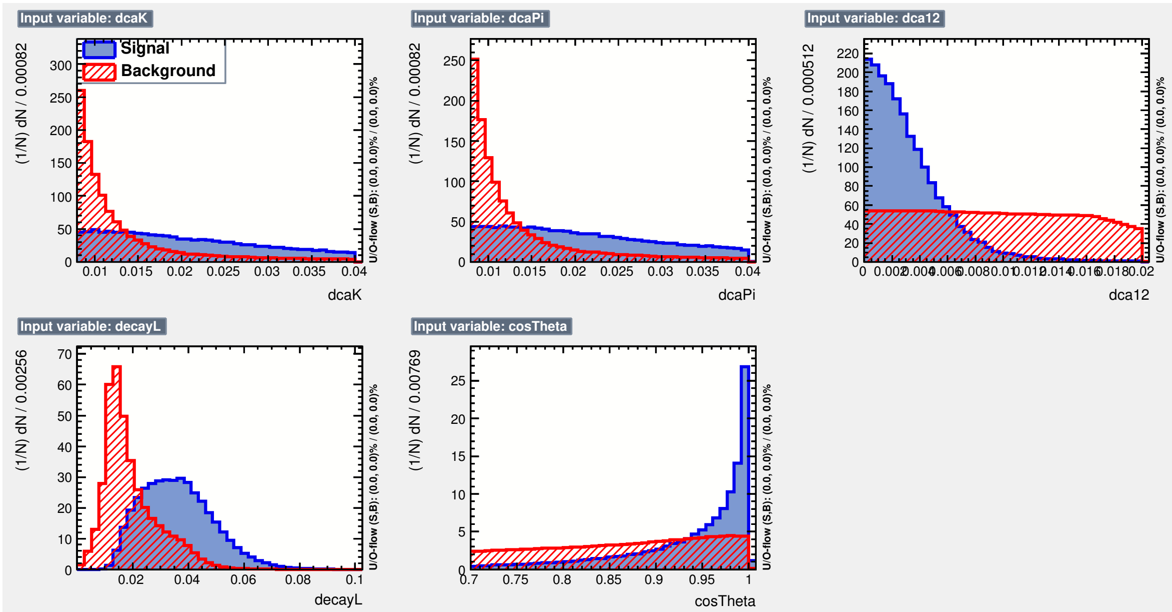

FIG. 17: Distributions of 5 topological variables for non-prompt D^0 signal (blue) and background (red) at 2-3 GeV/c, 0-10% collisions.

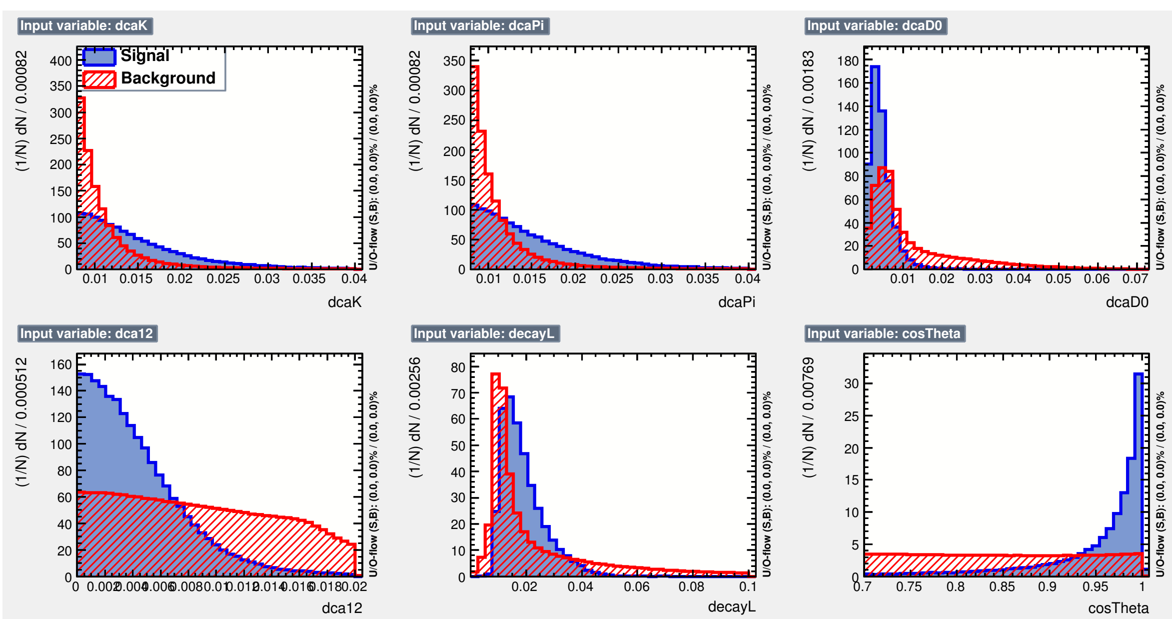

FIG. 18: Distributions of 5 topological variables for prompt D^0 signal (blue) and background (red) at 0-0.5 GeV/c, 0-10% collisions

and background (red) at $2 < p_T < 3$ GeV/c in 0-10% collisions.

Fig. 18 shows example distributions of 5 topological variables for prompt D^0 signal (blue) and background (red) at the lowest bin $0 < p_T < 0.5$ GeV/c in 0-10% collisions.

Fig. 19 shows signal efficiency, background efficiency, and significance etc. as a function of

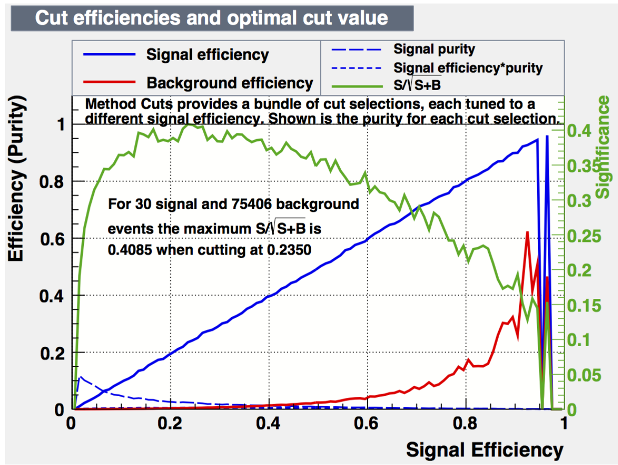

FIG. 19: Signal efficiency, background efficiency, and significance etc. as function of signal efficiency at 2-3 GeV/c, 0-10% for non-prompt D^0

signal efficiency at 2-3 GeV/c, 0-10% for non-prompt D^0. Significance is calculated for 1 million events. The wiggling distribution in significance is due to limited statistics used in the TMVA training, and can be smoothened by running more statistics in the training. But with more statistics in the input tree for TMVA, it will need more CPU time to train.

We choose the topological cuts with the best significance from TMVA training. The cuts are listed in Table. III for 0-10% and 0-80%, and Table. IV for 60-80%.

D^0 p_T (GeV/c)	0-1	1-2	2-3	3-4	4-5	5-7	7-10
DCA$_{D^0}(\mu m) <$ (only for prompt D^0)	50	50	50	50	60	60	70
DCA$_K(\mu m) >$	153	125	107	105	84	80	79
DCA$_\pi(\mu m) >$	165	140	116	140	92	89	81
$dcaDaughters(\mu m) <$	73	50	49	52	37	55	42
$decayLength(\mu m) >$	233	237	291	361	421	495	275
$cos\theta >$ (for non-prompt D^0)	0.85	0.88	0.97	0.98	0.98	0.987	0.99
$cos\theta >$ (for prompt D^0)	0.96	0.97	0.97	0.98	0.98	0.987	0.99

TABLE III: Prompt and non-prompt D^0 topological cuts at 0-10% and 0-80%

D^0 p_T (GeV/c)	0-1	1-2	2-3	3-4	4-5	5-7	7-10
$\mathrm{DCA}_{D^0}(\mu m) <$ (only for prompt D^0)	50	50	50	50	60	60	70
$\mathrm{DCA}_K(\mu m) >$	169	156	131	82	80	72	41
$\mathrm{DCA}_\pi(\mu m) >$	168	133	117	90	90	59	63
$dcaDaughters(\mu m) <$	67	64	49	45	45	67	200
$decayLength(\mu m) >$	182	216	275	292	293	424	196
$cos\theta >$ (for non-prompt D^0)	0.75	0.71	0.86	0.93	0.93	0.958	0.98
$cos\theta >$ (for prompt D^0)	0.95	0.95	0.95	0.95	0.96	0.96	0.98

TABLE IV: Prompt and non-prompt D^0 topological cuts at 60-80%

3-3. Correlated background estimation

Besides combined background (Mix-event Background), there are also residual correlated background contributions underneath the D^0 peak, especially at high p_T. Fig. 20 shows D^0 signal at $2 < p_T < 10$ GeV/c from STAR Run14 HFT. The Mix-event unlike-sign and same-event like-sign distributions both under-estimate the total background. The residual background mainly comes from double mis-PID, jet fragmentation and muti-prong D^0 or other D-meson decays (e.g. $K^-\pi^+\pi^0$).

It is not easy to estimate the full correlated background without imposing some physics model. In this study, we take a first order estimation based on the STAR HFT data. Fig. 21 shows D^0 correlated background to inclusive D^0 signal ratio as a function of D^0 p_T in 0-10% (left), 0-80% (middle), 60-80% (right) from the STAR HFT data. Black circles are with default topological cuts (default), red squares are with tight topological cuts ($\sim$ 50% efficiency compared to default) and blue stars are with loose topological cuts ($\sim$ 150% efficiency compared to default). There are some fluctuations, but to first order, one can see the correlated background yield has a correlation with the total signal yield. We parametrize the dependence with a linear function and add this additional background contribution to the total background in our estimation.

3-4. Results

In this simulation, we ran 1 billion events for 0-10% background, 5 billion events for 0-80% background and 50 billion events for 60-80% background. 200 million B-mesons and D^0 mesons

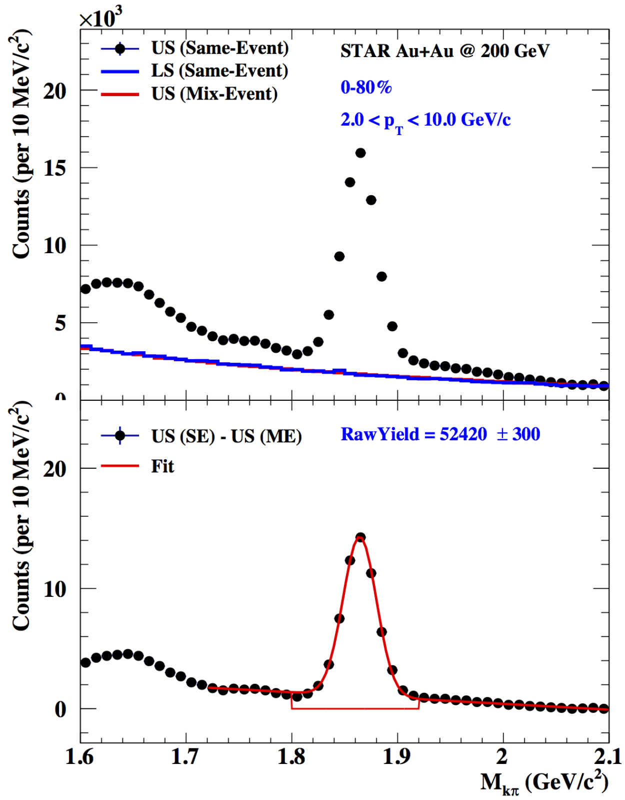

FIG. 20: D^0 signal from STAR Run14. (Top) full unlike-sign (US) same-event, like-sign (LS) same-event and US mixed-event distributions. (Bottom) Combinatorial background (US mixed-event method) subtracted US same-event distributions. The red box denote the D0 mass window which is excluded from the background fit.

are used to calculate signal efficiency and signal counts. At last, both signal and background are rescaled to 240 billion events for 0-100% minimum bias, 192 billion for 0-80%, 24 billion for 0-10%, and 48 billion for 60-80% to calculate significance, R_{CP}, v_2.

Fig. 22 shows an example of prompt and non-prompt D^0 invariant mass distributions. Fig. 23 shows an example of prompt and non-prompt D^0 DCA distributions. All distributions can be found at http://portal.nersc.gov/project/star/xlchen/sPhenix/sPhenix_note/PDF/.

In the following, all figures are within 3σ mass window ($1.82 < m_{K\pi} < 1.91$ GeV/c^2).

Fig. 24 show prompt (circle) and non-prompt (star) D^0 efficiencies in 0-10% (left), 0-80% (middle), 60-80% (right). Efficiency with ideal TOF PID is the same as without TOF.

Fig. 25 shows prompt (black circle) and non-prompt (black star) D^0 p_T spectra and their background (red circle, red star) in three centralities: 0-10% (left), 0-80% (middle), 60-80% (right) and three PID cases: without TOF (top), with TOF (middle), with ideal TOF (bottom). The back-

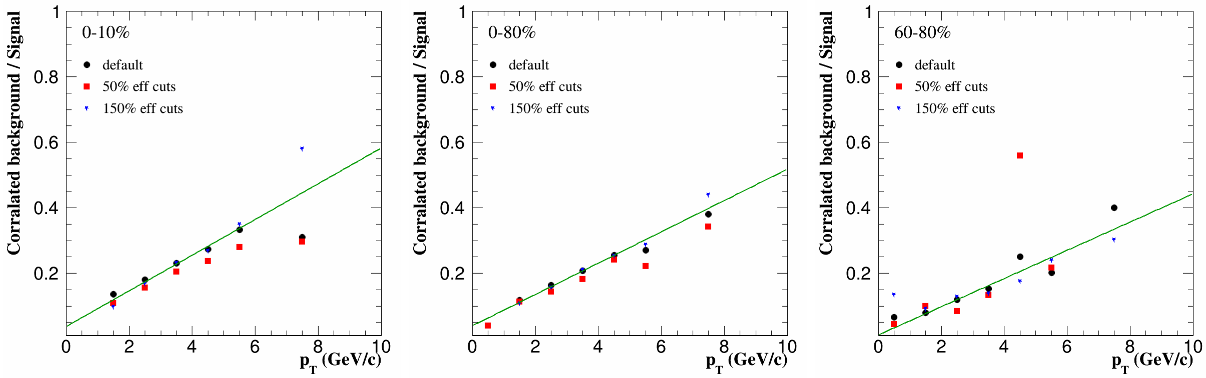

FIG. 21: D^0 correlated background over D^0 signal ratio as a function of D^0 p_T in three centralities: 0-10% (left), 0-80% (middle), 60-80% (right) from STAR HFT

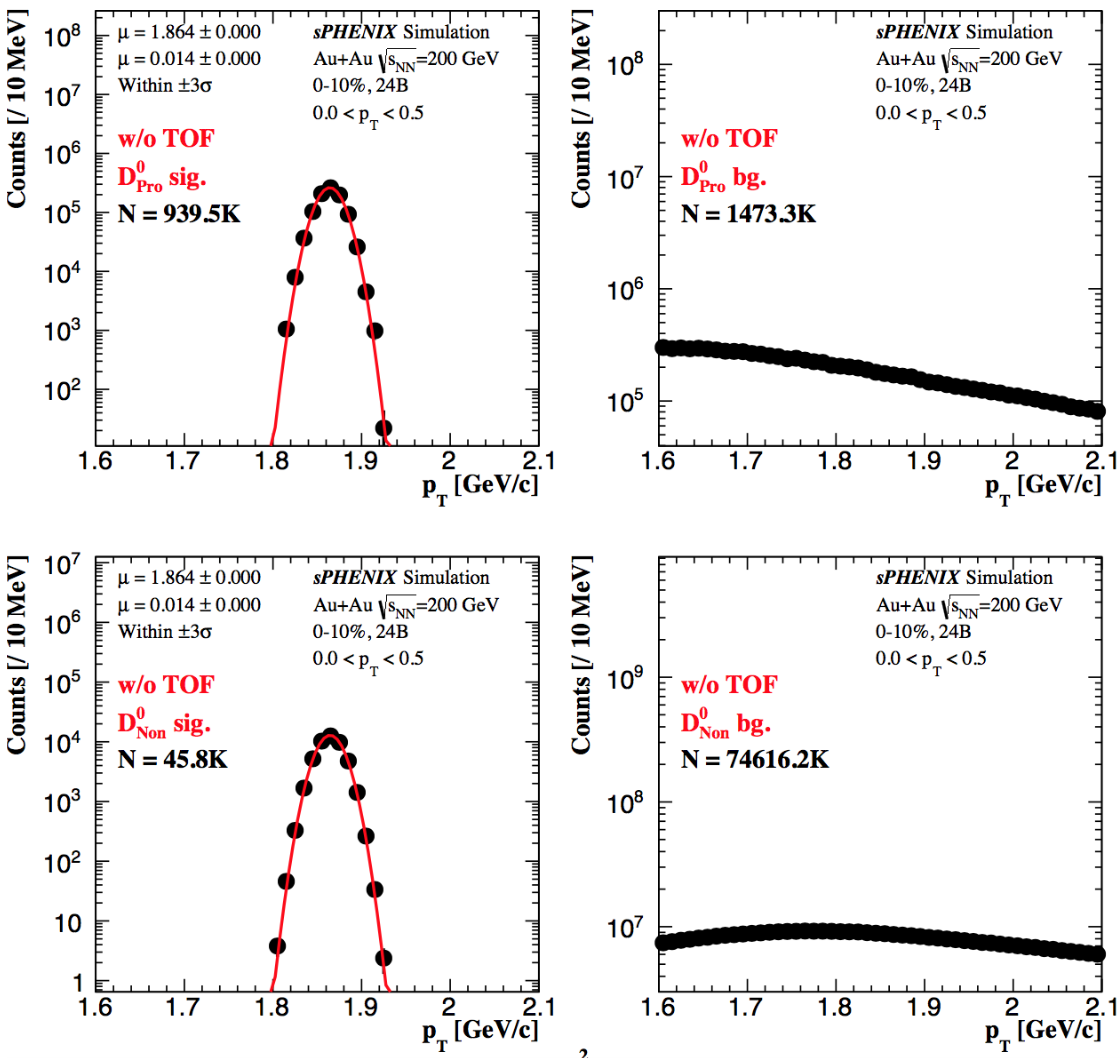

FIG. 22: Estimated D^0 invariant mass distributions for prompt signal (top left), prompt background (top right), non-prompt signal (bottom left) and non-prompt background (bottom right) in 0-0.5 GeV/c from 24B 0-10% central Au+Au collisions.

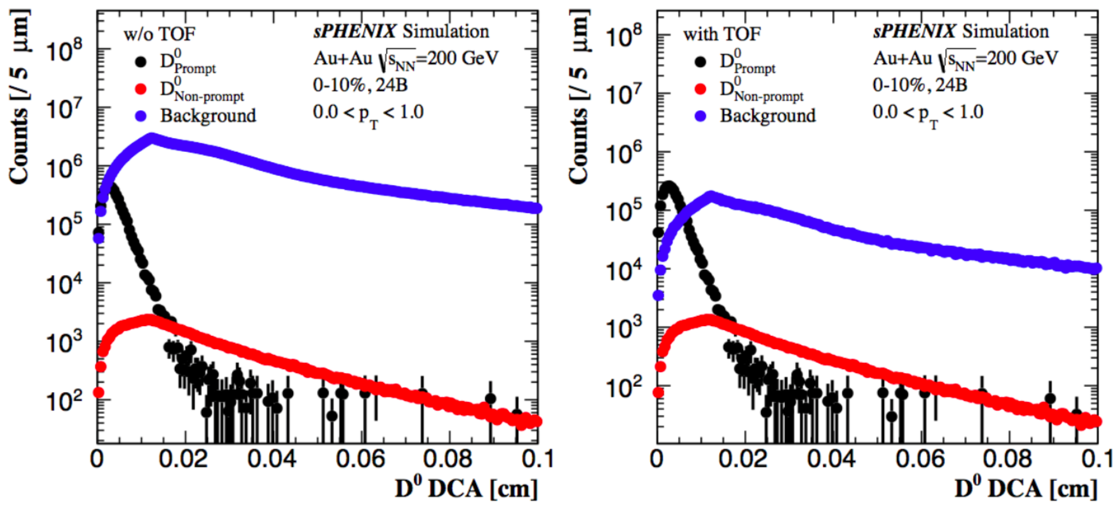

FIG. 23: Estimated D^0 DCA distributions for prompt, non-prompt and background from 24B 0-10% central Au+Au collisions for two cases: no PID on the left and TOF PID on the right.

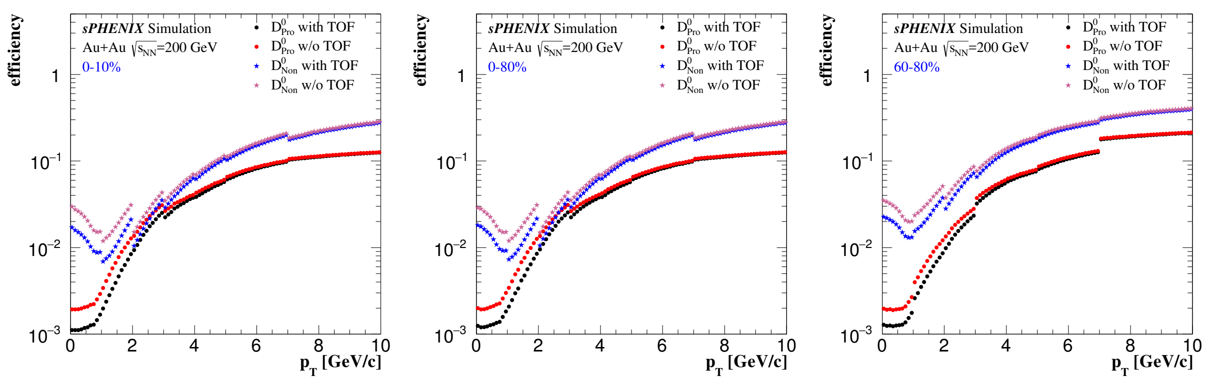

FIG. 24: Prompt (circle) and non-prompt (star) D^0 efficiency in three centralities: 0-10% (left), 0-80% (middle), 60-80% (right)

ground p_T distributions include combined background and correlated background in this figure.

Prompt and non-prompt D^0 significance are calculated for 24 billion 0-10% events, 192 billion 0-80% events (total 240 billion minimum bias), and 48 billion 60-80% events in Fig. 26. With TOF PID, non-prompt D^0 significance can be much improved. We considered the total background underneath the inclusive D^0 invariant mass as the background to non-prompt D^0 background for a conservative estimation.

The statistical uncertainties of prompt and non-prompt D^0 R_{CP} are calculated in Fig. 27. The theory curves are an average R_{AA} based on calculations from Duke, TAMU and CUJET [5, 6].

Fig. 28 shows the statistical uncertainty estimation of prompt and non-prompt D^0 v_2 measure-

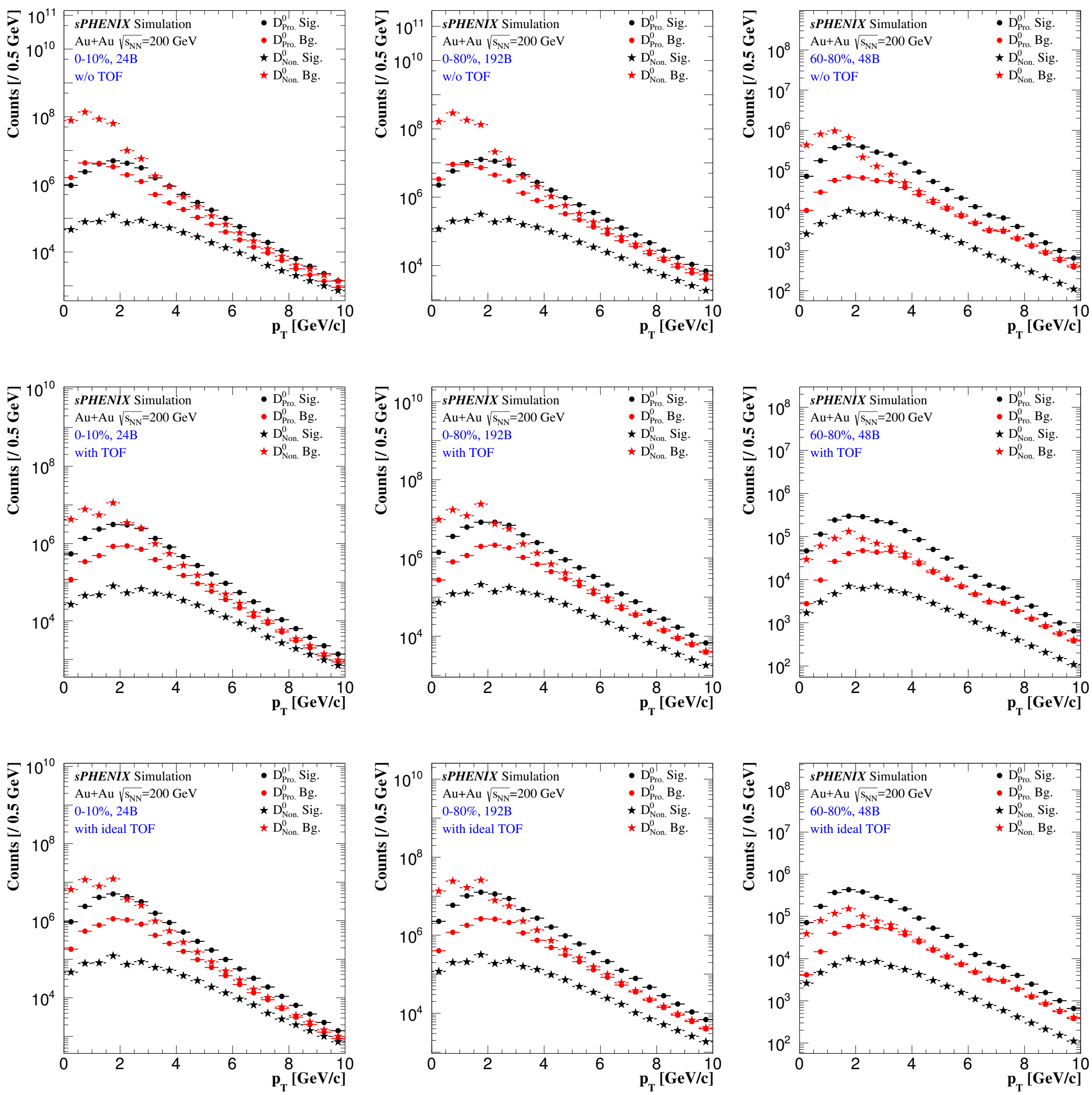

FIG. 25: Prompt (black circle) and non-prompt (black star) D^0 p_T spectra and their background (red circle, red star) in three centralities: 0-10% (left), 0-80% (middle), 60-80% (right) and three PID cases: without TOF (top), with TOF (middle), with ideal TOF (bottom)

ments. The statistics uncertainty on v_2 is calculated with Equation. 3. An additional 70% event plane resolution for 0-80% collisions is assumed in this calculation. The dashed blue line is a fit curve to the STAR HFT D^0 data points [9]. And the dotted dashed red line is assuming B-meson v_2 follows the same m_T scaling as light and charm hadrons.

$$err(v_2) = \frac{\pi}{4} \frac{\sqrt{1-(4v_2/\pi)^2}}{Significance \times Resolution} \tag{3}$$

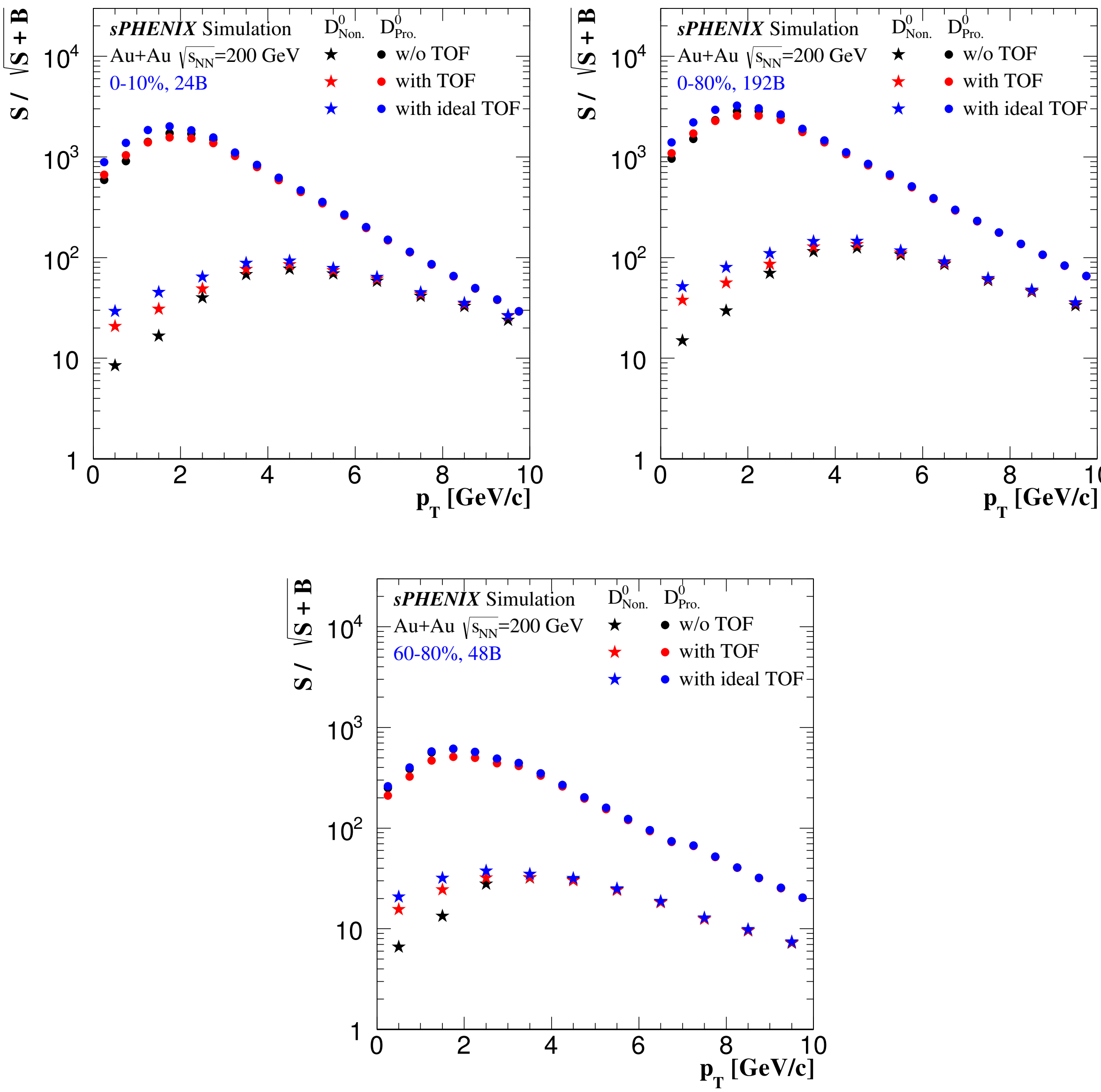

FIG. 26: Prompt (circle) and non-prompt (star) D^0 significance in three centralities: 0-10% (top left), 0-80% (top right), 60-80% (bottom) and three PID cases: without TOF (black), with TOF (red), with ideal TOF (blue)

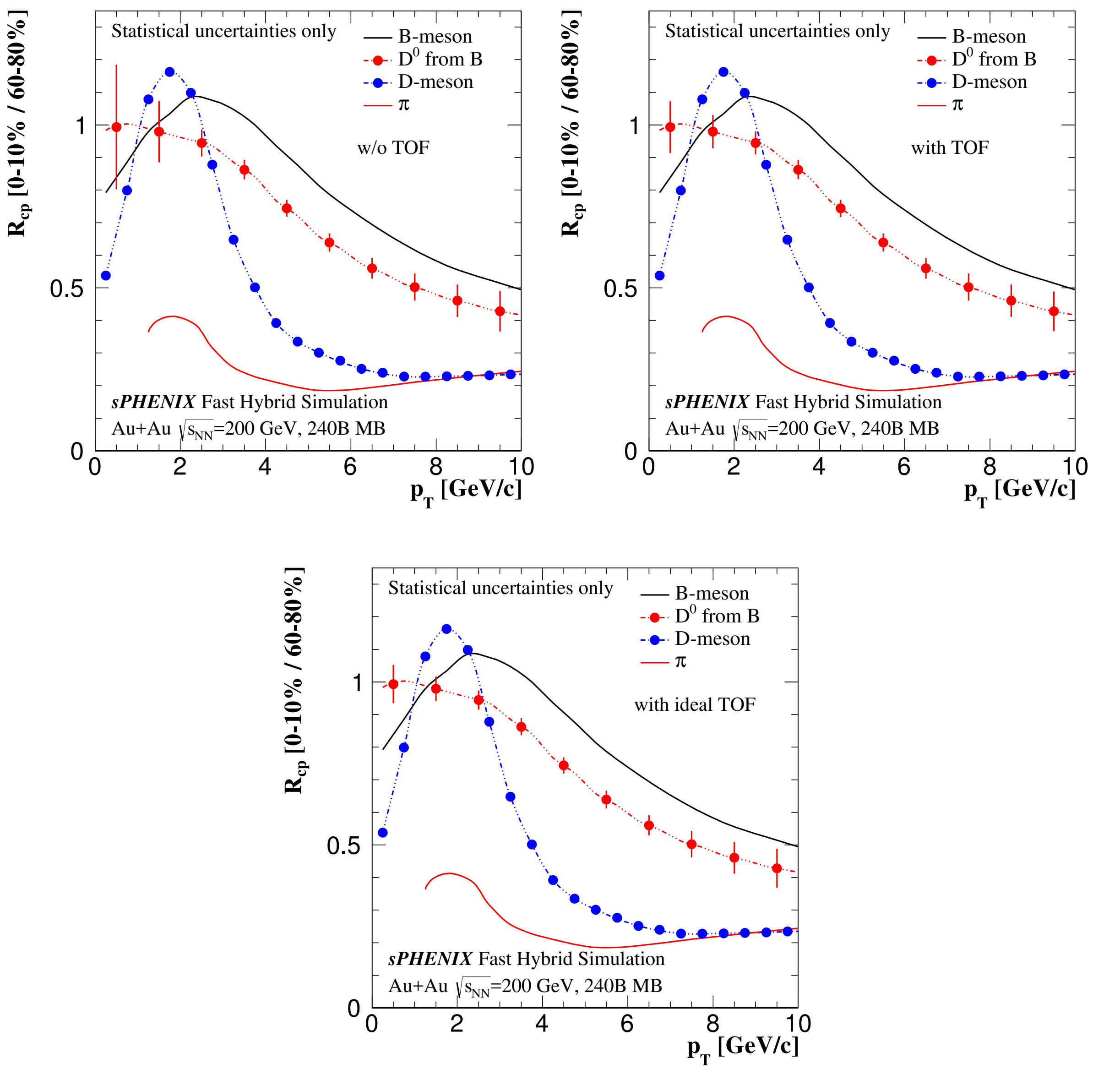

FIG. 27: Statistical uncertainty projection for prompt (blue circle) and non-prompt (red circle) D^0 R_{CP} measurements in three PID cases: without TOF PID (top left), with TOF PID (top right), with ideal TOF PID (bottom)

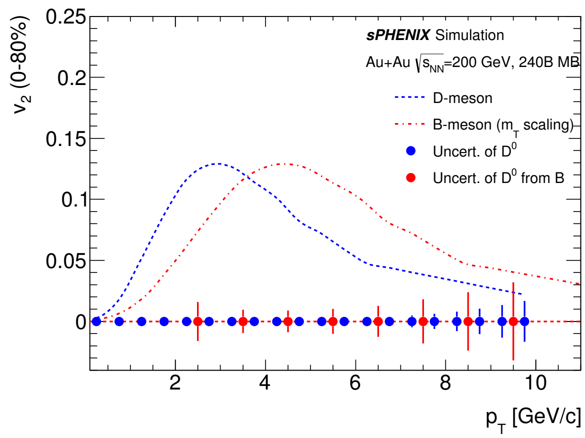

FIG. 28: Statistical uncertainty projection for prompt (blue circle) and non-prompt (red circle) D^0 v_2 from 240B 0-100% minimum bias events. The v_2 measurement is assumed to be carried out in the centrality bin 0-80%.

4. B^+ MEASUREMENT

In this section, we will introduce the direct B^+ reconstruction through the $\bar{D}^0\pi^+$ channel:

$b\bar{b} \to B^{\pm}$, F.R. = 0.4

$B^+ \to \bar{D}^0\pi^+$, B.R. = 0.00481

$D^0 \to K^-\pi^+$, B.R. = 0.0388

4-1. Signal and combinatorial background simulation

The basic procedure for B^+ signal and background simulation is same as described in Section. 2 2-2.

For the signal simulation, we throw B^+ with a distribution flat in p_T from 0 to 20 GeV/c, flat in y from -1 to 1, flat in ϕ from 0 to 2π distributions are used as the input. We then apply the p_T shape weight based on FONLL calculations multiply some pre-assumed R_{AA} factors(Fig. 14). The total B^+ cross section is calculated using the $b\bar{b}$ cross section from FONLL $\times$ R_{AA} $\times$ N_{bin} $\times$ 0.4 (F.R.) $\times$ 0.00481 (B.R.: $B^+ \to \bar{D}^0\pi^+$) $\times$ 0.0388 (B.R.: $D^0 \to K^-\pi^+$) (Table. II). $B^{\pm}$ is forced to decay to $D^0\pi$ with 100% branch ratio, and D^0 is forced to decay to kaon and pion with 100% branch ratio to enhance the statistics

Background simulation is similar to D^0, but taking three-particle (k, π, π) random combinations. We consider here $K\pi\pi$ random combinations only.

We simulated two centrality classes: 0-80% and 0-10%. We assume the sPHENIX detector performance at 0-80% is the same with that at 0-10% (Section. 2 2-1) as a conservative estimate.

In each centrality, we simulated two kinds of PID methods to reconstruct signal and background. Single particle PID is defined at Section. 2 2-2.

1. **w/o TOF** : no PID for all K, π, p final state particles. Kaon sample, pion sample 1 and 2 will include all kaons/pions/protons.

2. **with TOF** : Assuming TOF matching efficiency from STAR Run14 data (Fig. 8). Kaon sample apply hybrid PID, it will include all kaons, part of pions $(1 - tofMatch\_\pi)$, and part of protons $(1 - tofMatch\_P)$. Two pion samples also apply hybrid PID and will include all pions, part of kaons $(1 - tofMatch\_K)$, and part of protons $(1 - tofMatch\_P)$. Signal also won't lose efficiency from TOF match. But due to TOF PID, kaon sample and two pion samples will decrease some mis-identified particles.

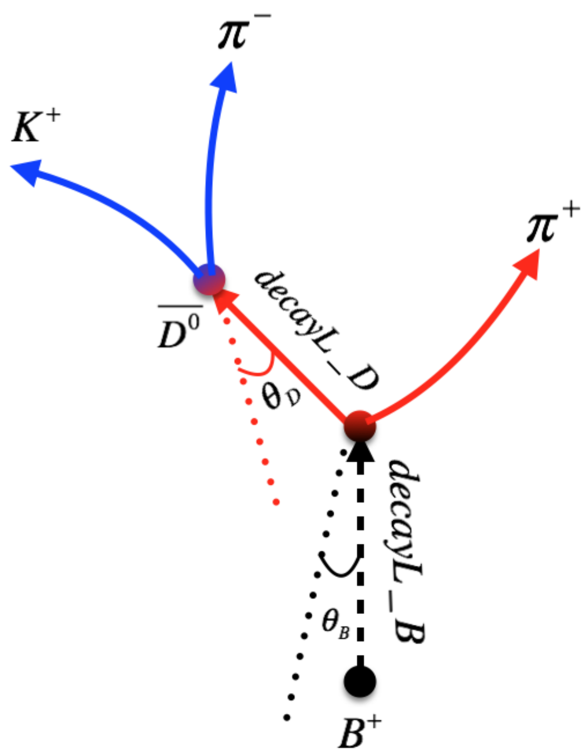

FIG. 29: Cartoon of prompt B^+ decay structure

4-2. Topology cuts tuning

The basic K/π cuts we used for B^+ reconstruction are: $p_T > 0.6$ and $|\eta| < 1$.

Fig. 29 is a cartoon of prompt B^+ decay structure. It has two decay vertices, one is from $B^+ \to \bar{D}^0\pi^+$, the other is from $\bar{D}^0 \to K^+\pi^-$. There are total 11 topological variables related to the two decay vertices:

- $dcaK$: the Distance of Closest Approach from K track to PV (Primary Vertex).
- $dcaPi1$: The Distance of Closest Approach from π (from D^0) track to PV.
- $dcaPi2$: The Distance of Closest Approach from π (from B^+) track to PV.
- $dcaD0$: The Distance of Closest Approach from D^0 track to PV.
- $dcaB$: The Distance of Closest Approach from B^+ track to PV.
- $dca12$: DCA between K and π (from D^0).
- $dca123$: DCA between D^0 and π (from B^+).

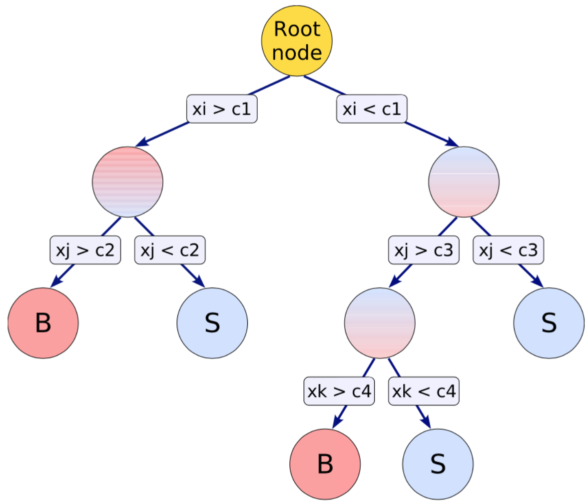

FIG. 30: Decision tree structure

- $decayL_B$: B^+ decay length.
- $decayL_D$: D^0 decay length.
- $cosThetaB$: $cos\theta_B$, see the cartoon picture.
- $cosThetaD$: $cos\theta_D$, see the cartoon picture.

This list has 11 variables; however, since one of them is the $\mathrm{DCA}_B = decayL_B \times sin\theta_B$, so indeed we have 10 topological variables. In addition, $decayL_D$ from signal and background have similar distributions. At last we apply a simple $cos\theta_D > 0$, and choose 8 topological variables (excluding $dcaB$, $decayL_D$, and $cos\theta_D$) and D^0 p_T, totally 9 variables for cut tuning. (D^0 p_T can be removed and apply fixed cut range, this should have small difference.)

We choose the Boosted Decision Tree (BDT) method in TMVA package to tune the 9 variables. A decision tree looks like Fig. 30. It take different cuts on one variable at a time until a stop criterion is fulfilled. Then it splits the phase space into many regions that are eventually classified as signal or background, depending on the majority of training events that end up in the final leaf node. The boosted decision tree means using several decision trees (forest), and the weighted average of these tree decisions as the only output (BDT response).

We only studied the tuning for the 0-80% centrality no PID case. We apply the same tuned result to other cases (0-80% with TOF, 0-10% etc.). For training, we ran 110 billion events for background and 20 million B^+. The signal and background are both rescaled to 240 billion events. The input tree for TMVA package is within 3σ mass window both for D^0 and B^+ ($1.82 < m_{D^0} <$

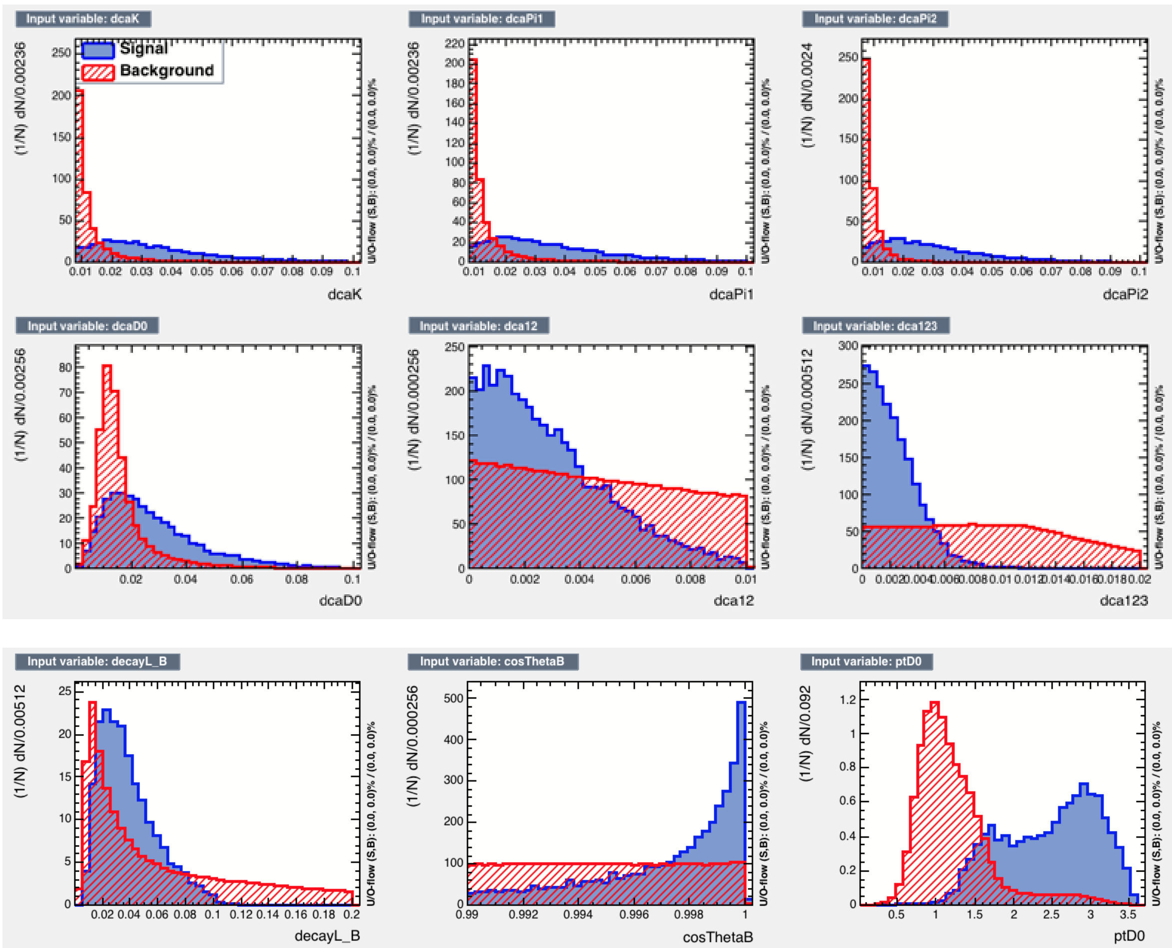

FIG. 31: Distributions of 9 tuned variables for B^+ signal (blue) and background (red) at 1-2 GeV/c, 0-80%

1.91 GeV/c^2, $5.16 < m_{B^+} < 5.40$ GeV/c^2) both for signal and background. And we also apply some initial cuts to make input tree smaller to save CPU time.

Fig. 31 show example distributions for the 9 tuned variables for B^+ signal (blue) and background (red) at 1-2 GeV/c, 0-80%.

Fig. 32 shows the BDT response for signal and background, and overtraining check at 1-2 GeV/c. It shows very good separation between signal and background and no clear overtraining. The printed signal (background) probability in the figure means BDT response difference between two data samples (train sample and test sample). If the numbers are close to 0 (such as <0.05), it's a hint of overtraining. Some further check can be done by running more data samples to see whether the BDT response keeps stable.

Fig. 33 shows the signal efficiency, background efficiency, and significance etc. as function of signal efficiency at 1-2 GeV/c, 0-80% for B^+. Significance line is calculated with 100 billion

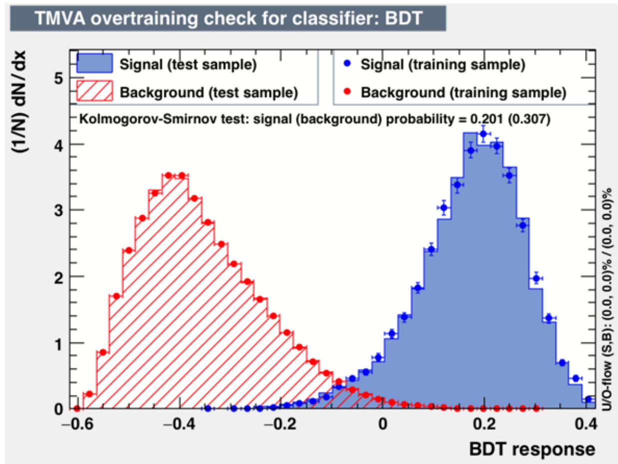

FIG. 32: BDT response and over training test at 1-2 GeV/c, 0-80% for B^+

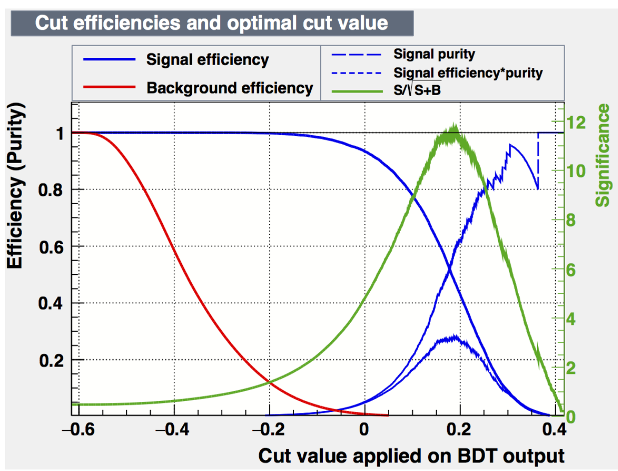

FIG. 33: Signal efficiency, background efficiency, and significance etc. as function of signal efficiency at 1-2 GeV/c, 0-80% for B^+

events.

4-3. Results

We ran 6 billion events for 0-10% background, 110 billion events for 0-80% background. 30 million B^+-mesons for 0-10% and 0-80% are ran respectively to calculate signal efficiency and signal counts. At last, both signal and background are normalized to 192 billion events for 0-80% (total 240 billion mimimum bias), 24 billion events for 0-10% to calculate B^+ significance.

Fig. 34 shows re-sampled B^+ (signal + background) invariant mass distributions based on the estimated signal and background counts in 24B 0-10% Au+Au 200 GeV events without TOF PID. In our simulation sample, we parametrize the background and signal distributions with linear and

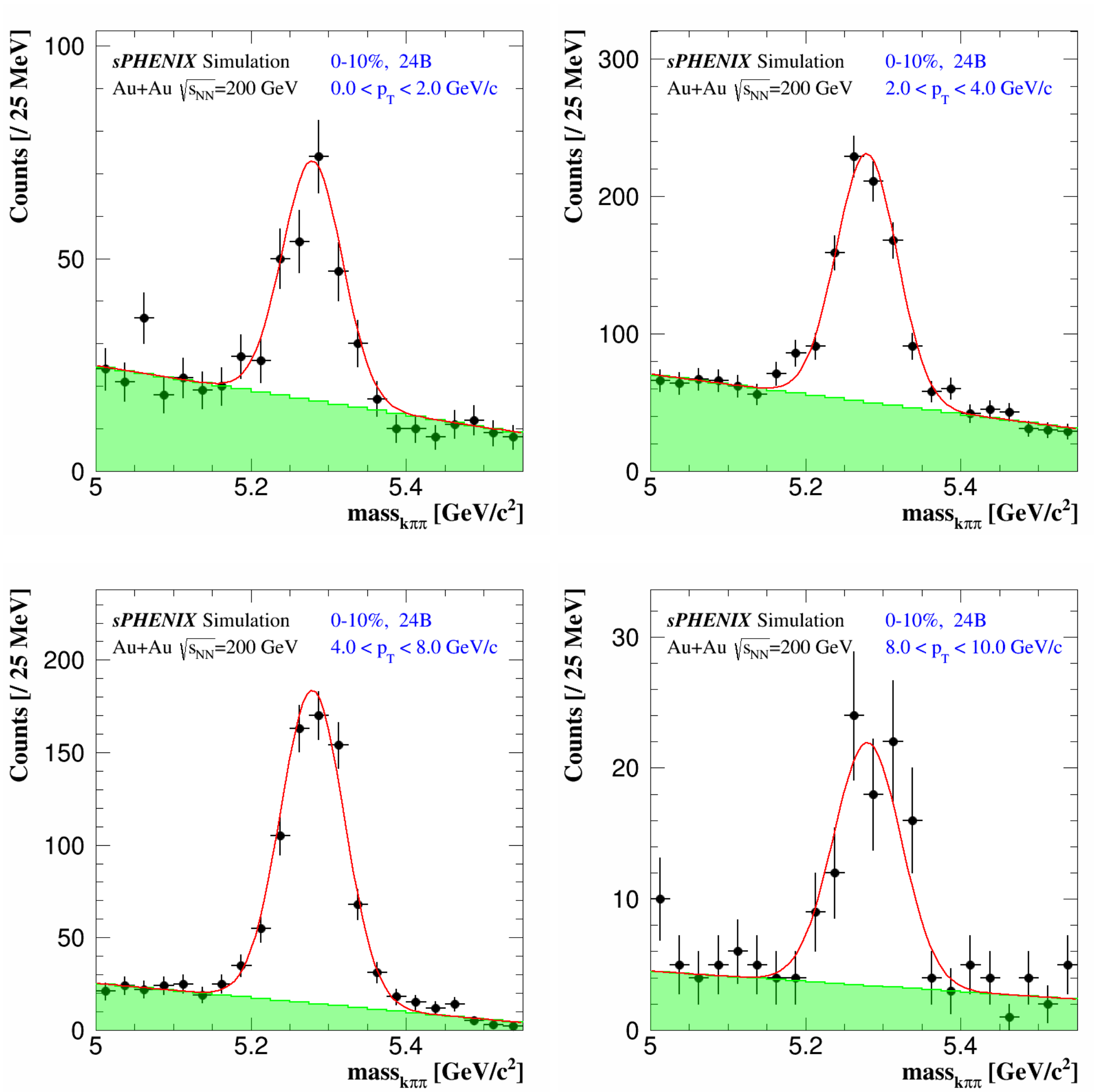

FIG. 34: Re-sampled B^+ (signal + background) invariant mass distributions

Gaussian fits, respectively. To emulate the anticipated B^+ signal, we re-sample each data point according to the fit function assuming Poisson statistics. All signal and background fitting and re-sampling at different p_T bins and centralities can be found at http://portal.nersc.gov/project/star/xlchen/sPhenix/sPhenix_note/PDF/.

Fig. 35 shows the B^+ efficiency in 0-10% (left), 0-80% (right). Efficiency with TOF is the same as without TOF because we use hybrid TOF PID.

In the following, all panels show results for selections within 3σ mass window both for D^0 and B^+ ($1.82 < m_{D^0} < 1.91$ GeV/c^2, $5.16 < m_{B^+} < 5.40$ GeV/c^2).

Fig. 36 shows B^+ p_T spectra (black circle) and their background (red circle) in two centralities:

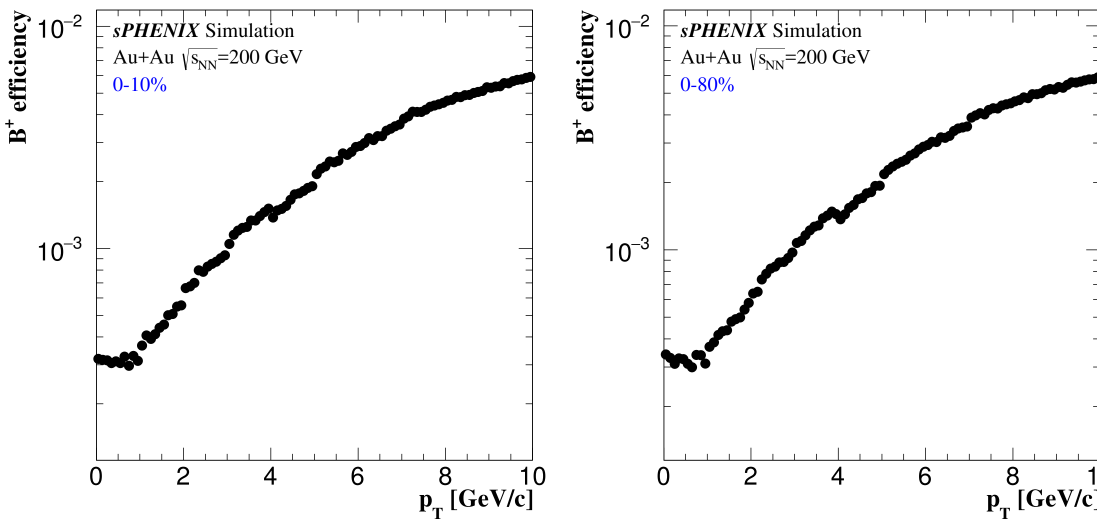

FIG. 35: B^+ efficiency in 0-10% (left), 0-80% (right)

0-10% (left), 0-80% (right) and two PID cases: without TOF (top), with TOF (bottom).

B^+ significance values calculated for 24 billion 0-10% events and 192 billion 0-80% events (total 240 billion mimimum bias events) are shown in Fig. 37. Due to the powerful topological reconstruction for such cascading decays, the background level is mostly less compared to signal yield (Fig. 36). And there is no big difference in B^+ significance with and without TOF PID.

4-4. Discussion on other background contribution

One more combinatorial background can come from D^0+π random combination. However, this contribution can be largely suppressed due to typical $\mathrm{DCA_{D^0}}$ cut to require off-vertex decays. In our simulation, since we used the TMVA BDT method, what is applied is not a sharp cut in $\mathrm{DCA_{D^0}}$. Figure 38 left panel shows the D^0 DCA distributions for reconstructed B^+ signal and combinatorial background after topological cuts applied. One can see the topological cut effectively remove low DCA_{D^0} candidates. The right panel of Figure 38 shows the simulated DCA_{D^0} for total prompt D^0, non-prompt D^0 and combinatorial background as studied in section 3 in the same p_T bin before any further B^+ topological reconstruction. One can expect with the effective DCA_{D^0} cut, the prompt D^0 that peaks close to zero will be significantly removed. To have a more quantitative estimation, we plan to run also fast MC to include this contribution in the near future.

Another background source is the correlated background from B-hadron multi-prong decays,

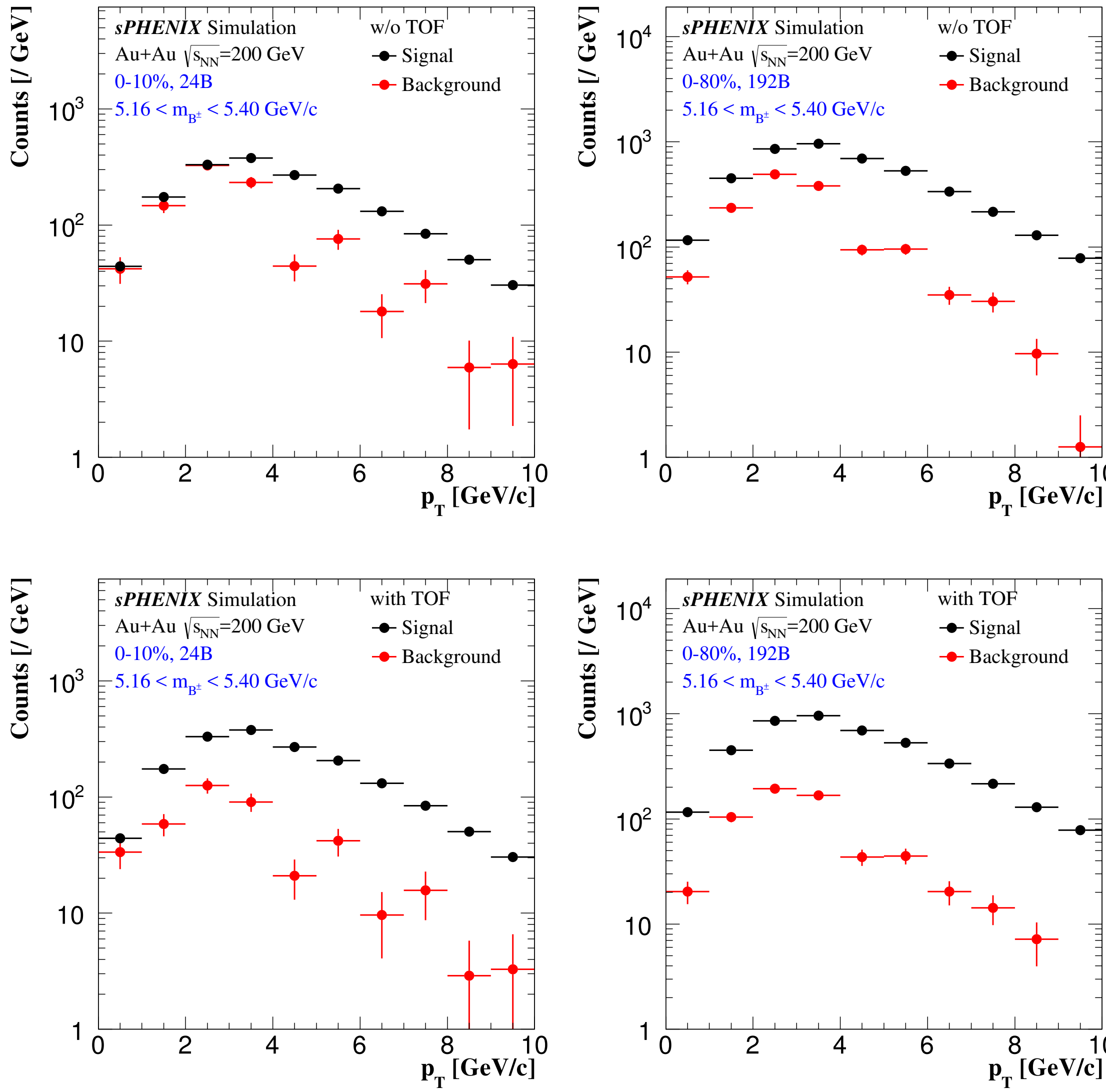

FIG. 36: B^+ p_T spectra (black circle) and their background (red circle) in two centralities: 0-10% (left), 0-80% (right) and two PID cases: without TOF (top), with TOF (bottom)

while we only reconstruct partially the D^0+π invariant mass. Usually these reconstructions miss one or more hadrons in the final states, so the invariant mass of D^0+π will be at least one pion mass lower than the expected B^+ mass. They will generate mostly correlated background or even some peak structure to the left of the fully reconstructed B^+ mass peak, and the signal from such a partial reconstruction will have an invariant mass distribution spreaded down to further lower mass region due to the momentum carried out by the missing pion. Figure 39 shows the invariant mass distributions from partial reconstruction in the channel $B^+ \rightarrow \overline{D^0}\rho^+ \rightarrow \overline{D^0}\pi^+\pi^0$ while missing a pion in the final state (green histograms). They are compared to the full B^+ invariant

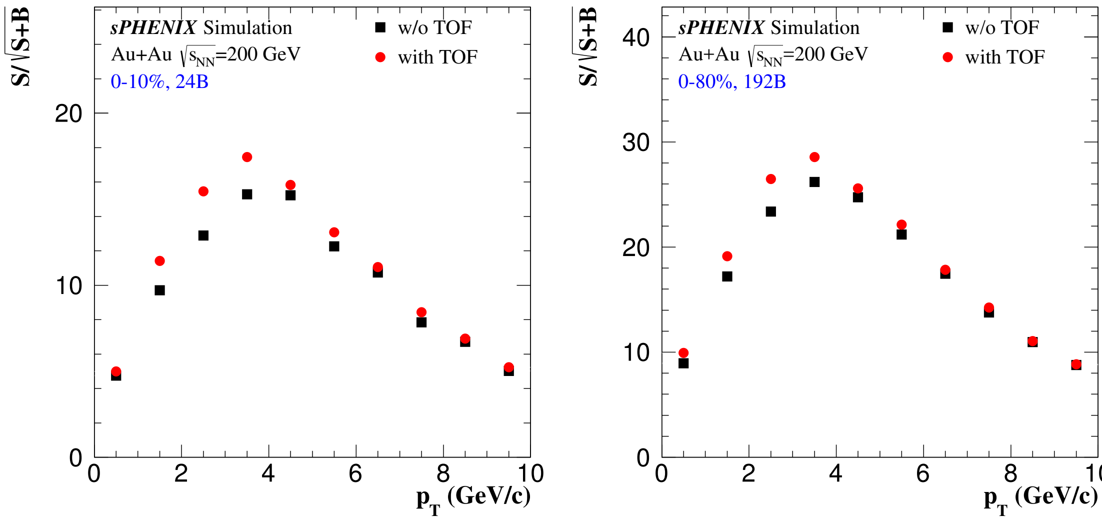

FIG. 37: B^+ significance in two centralities: 0-10% (left), 0-80% (right) and two PID cases: without TOF (black), with TOF (red)

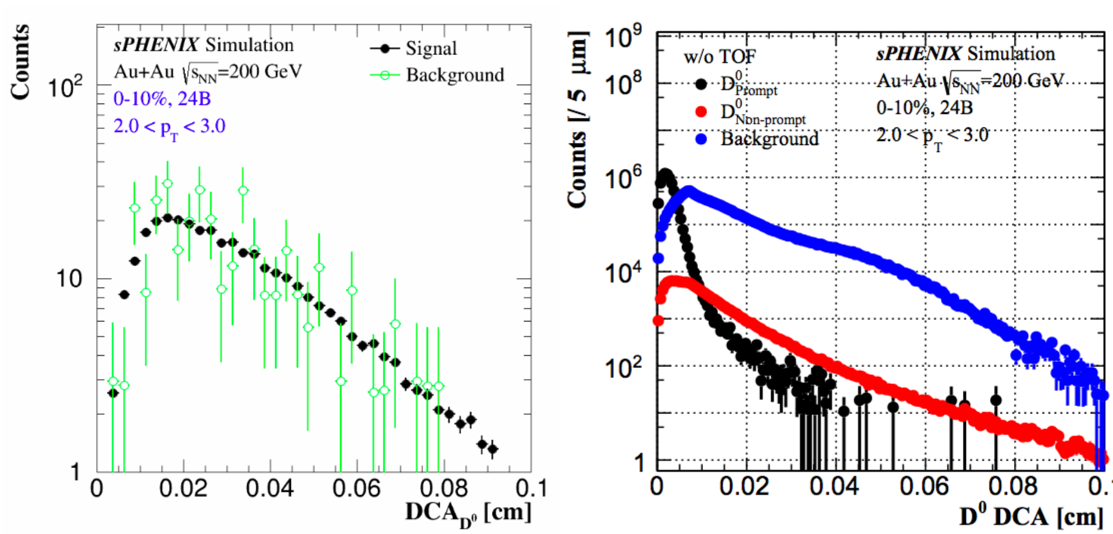

FIG. 38: (Left) D^0 DCA distributions for reconstructed B^+ signal and combinatorial background after topological cuts applied. (Right) D^0 DCA distributions for prompt D^0, non-prompt D^0 and combinatorial background as studied in section 3 in the same p_T bin before any further B^+ topological reconstruction

mass distributions and one can see the partial reconstruction in this channel only starts to affects the tail of the B^+ peak a bit. We plan to include more decay channels and investigate more detail other correlated contributions in the future.

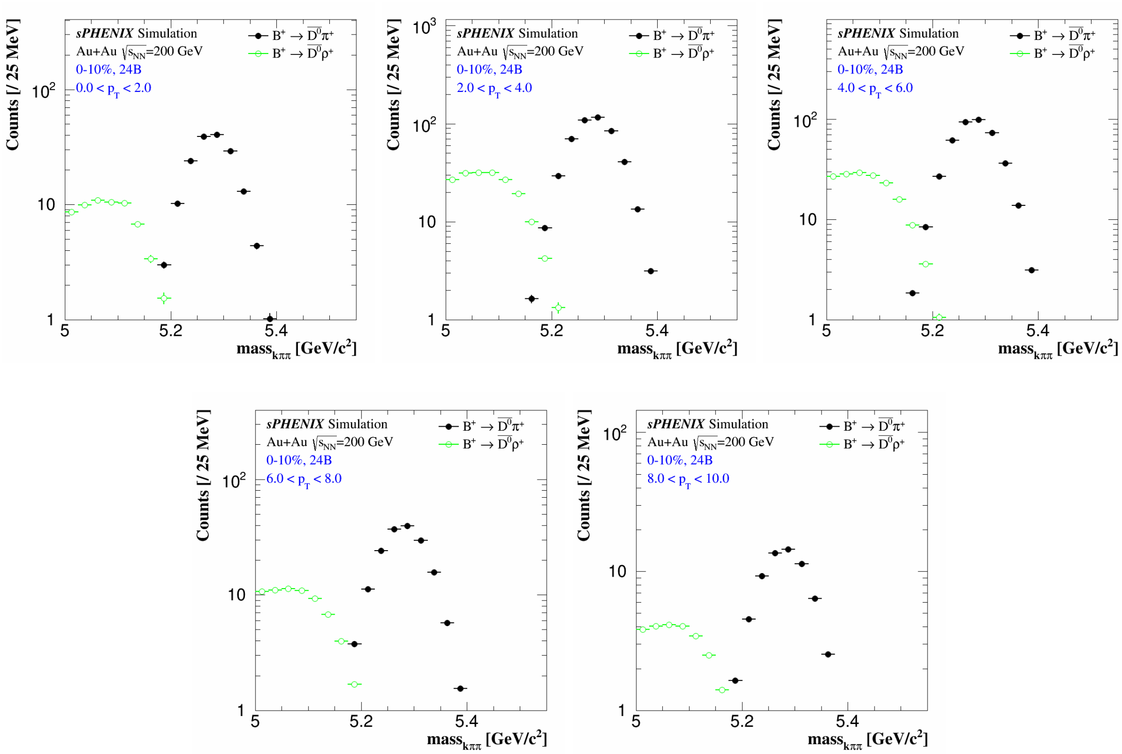

FIG. 39: Invariant mass distributions from partial reconstruction in the channel $B^+ \rightarrow \overline{D^0}\rho^+ \rightarrow \overline{D^0}\pi^+\pi^0$ while missing a pion in the final state (green histograms) compared to the full $B^+ \rightarrow \overline{D^0}\pi^+$ reconstructed invariant mass distributions in central collisions in various p_T bins.

5. COMMENT ON THE LOWEST p_T BIN

There is a concern that whether we are able to reconstruct the D^0 at the lowest p_T bin (0-0.5 GeV/c) since these D^0-mesons decay mostly very close to the collision vertex. Here let us walk through the numbers to have a sense on the estimated statistic errors.

The number of D^0s in the 0-0.5 GeV/c p_T bin that decay through the $K\pi$ channel from 24B 0-10% central Au+Au collisions is $0.17/42 * 1000 * 2 * 2 * 0.6 * 0.15 * 24e9 * 0.039 = 1.4e9$

- 0.17 mb - $d\sigma/dy$ for $c\bar{c}$ pair production cross section in $p+p$ collisions at 200 GeV from the STAR measurement [10]. The PHENIX value [11] is about 30% lower than the STAR measured value.
- 42 mb - total pp inelastic scattering cross section at 200 GeV.
- 1000 - N_{bin} for central Au+Au collisions 0-10%.
- 2 - counting y from -1 to 1
- 2 - counting both charge signs
- 0.6 - $c \to D^0$ fragmentation fraction.
- 0.15 - fraction of D^0 yield in the p_T region of 0-0.5 GeV/c over the total p_T integrated yield.
- 24e9 - 24B 0-10% central Au+Au events
- 0.039 - $D^0 \to K^-\pi^+$ decay branching ratio

They are billions of signals expected in this p_T bin. In order to reconstruct the D^0 signal, one has to apply reasonable topological cuts to separate the decays aways from primary vertex. Since these D^0 decay very close to the vertex, this means the topological cuts, if kept no big difference w.r.t other p_T bins, will yield a small acceptance*efficiency. In other words, we are reconstructing also mostly these D^0 that decay in their decay length tails. Figure 40 shows the estimated efficiencies (including acceptance) from several different components.

The acceptance here is defined as daughter p_T and η cut acceptance. The dip around 1 GeV/c is caused by the daughter $p_T > 0.6$ GeV/c cut (we will address this cut in a separated response). For the lowest p_T bin, the tracking and acceptance together will contribution roughly 0.4*0.4 $\sim$ 0.16 to the total efficiency.

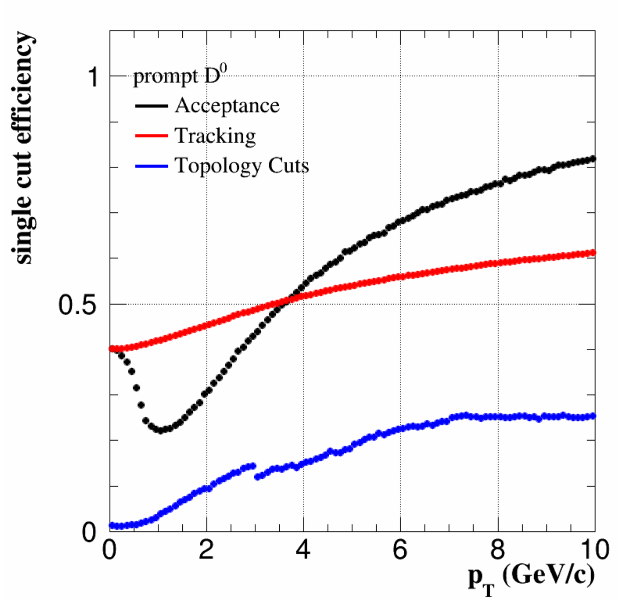

FIG. 40: D^0-meson reconstruction efficiency as a function of p_T with each component contribution separated in central Au+Au collisions for sPHENIX.

In the figure, it also shows the topological cut efficiency (including decay length cut acceptance certainly) is about 10^{-2} in the lowest p_T bin. One can see clearly the increasing trend of this efficiency as a function of p_T mostly due to the D^0 boost so we will be accepting more D^0 at higher p_T.

The total efficiency is on the order of 10^{-3} when combining three components together. This leads to the final reconstructed signal yields to be around 10^6, as shown in Figure 25. With such topological cuts, the S/B ratio is around 1/2 in this lowest p_T bin for the reconstructed D^0-mesons.

Figure 27 and 28 show the estimated statistical uncertainty projection for R_{CP} and v_2 for these measurements. The significance for prompt D^0-mesons is very good in such a large dataset. The systematic uncertainties that are associated with these measurements are to be investigated.

For the spectra analysis, there are two major systematic sources. One is coming from the signal yield extraction. Considering the S/B ratio is very reasonable even in the lowest p_T bin, it also makes sense to assume that the systematic error associated with the raw yield reconstruction should be under control. Figure 41 shows the reconstructed D^0 signal from the STAR HFT out of 900M mb events. With the anticipated sPHENIX MVTX performance as well as the large dataset we aim to collect, a reasonable D-meson reconstruction in the lowest p_T bin should be reliable.

One remaining question is the uncertainty associated with the efficiency*acceptance correction that eventually will be translated into the uncertainty in the final spectra. The estimation will be

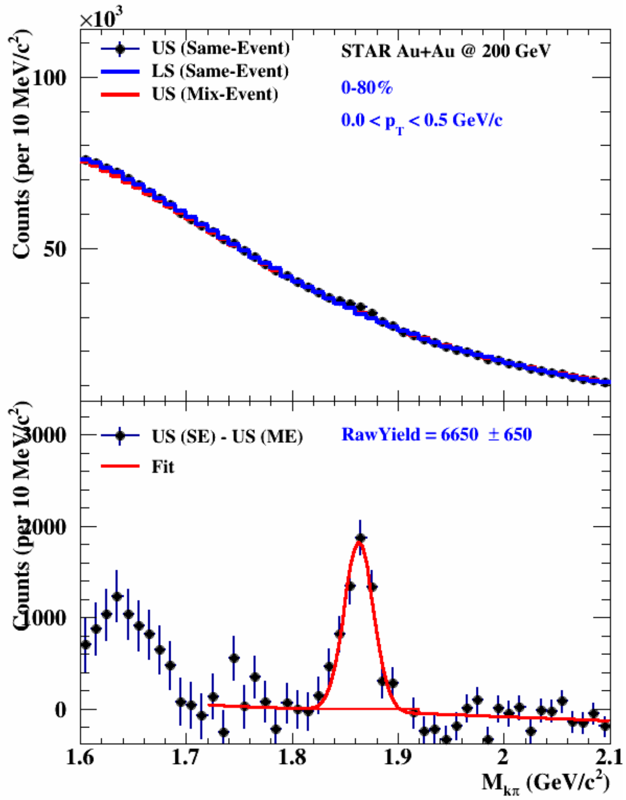

FIG. 41: STAR measured D^0-meson signal in the p_T region of 0-0.5 GeV/c in 900M minimum bias Au+Au collisions.

a bit challenging since it will strongly depend on the real detector performance and how well our simulation can describe the real data. What we plan to do in the future is to implement some assumptions in terms of the agreement level between data and simulation and to estimate how these will modify the final efficiency corrected yield, therefore the systematic uncertainties from this source.

6. SUMMARY

The next phase of heavy quark program will be focusing on precision open bottom measurements to systematic investigate the mass hierarchy of parton energy loss and to precisely determine the QGP medium transport parameter - heavy quark diffusion coefficient $D_{HQ}(T)$. With sPHENIX MVTX detector, we have shown that we can conduct precise measurements of non-prompt D^0 (from B-meson decays) R_{CP} and v_2 in the range of $2 < p_T < 8$ GeV/c. We also studied the B-hadron reconstruction via the exclusive $\bar{D}^0\pi$ channel in the p_T region up to $\sim$10 GeV/c. The requested statistics are 240 billion 0-100% minimum bias trigger Au+Au events at $\sqrt{s_{NN}}$ = 200 GeV which will be collected in three Au+Au RHIC runs in the period of 2022-2026.

[1] "A monolithic active pixel sensor detector for the sphenix experiment." [Online]. Available: https://www.phenix.bnl.gov/WWW/publish/mxliu/sPHENIX/MVTX/sPHENIX-MVTX-Preproposal-022017-final.pdf

[2] B. Abelev, M. Aggarwal, Z. Ahammed, B. Anderson, D. Arkhipkin, G. Averichev, Y. Bai, J. Balewski, O. Barannikova, L. Barnby *et al.*, "Systematic measurements of identified particle spectra in pp, d+ au, and au+ au collisions at the star detector," *Physical Review C*, vol. 79, no. 3, p. 034909, 2009.

[3] G. Agakishiev, M. Aggarwal, Z. Ahammed, A. Alakhverdyants, I. Alekseev, J. Alford, B. Anderson, C. Anson, D. Arkhipkin, G. Averichev *et al.*, "Strangeness enhancement in cu-cu and au-au collisions at s n n= 200 gev," *Physical Review Letters*, vol. 108, no. 7, p. 072301, 2012.

[4] B. Abelev, M. Aggarwal, Z. Ahammed, B. Anderson, M. Anderson, D. Arkhipkin, G. Averichev, Y. Bai, J. Balewski, O. Barannikova *et al.*, "Identified baryon and meson distributions at large transverse momenta from au+ au collisions at s n n= 200 gev," *Physical review letters*, vol. 97, no. 15, p. 152301, 2006.

[5] S. Cao, G.-Y. Qin, and S. A. Bass, "Energy loss, hadronization, and hadronic interactions of heavy flavors in relativistic heavy-ion collisions," *Physical Review C*, vol. 92, no. 2, p. 024907, 2015.

[6] A. Andronic, F. Arleo, R. Arnaldi, A. Beraudo, E. Bruna, D. Caffarri, Z. C. Del Valle, J. Contreras, T. Dahms, A. Dainese *et al.*, "Heavy-flavour and quarkonium production in the lhc era: from proton–proton to heavy-ion collisions," *The European Physical Journal C*, vol. 76, no. 3, p. 107, 2016.

[7] M. Cacciari, "Fonll heavy quark production." [Online]. Available: http://www.lpthe.jussieu.fr/~cacciari/fonll/fonllform.html

[8] A. Hoecker, P. Speckmayer *et al.*, "Tmva package." [Online]. Available: http://tmva.sourceforge.net/

[9] L. Adamczyk, J. K. Adkins, G. Agakishiev, M. M. Aggarwal, Z. Ahammed, N. N. Ajitanand, I. Alekseev, D. M. Anderson *et al.*, "Measurement of D^0 azimuthal anisotropy at midrapidity in $\mathrm{Au}+\mathrm{Au}$ collisions at $\sqrt{s_{NN}} = 200$ GeV," *Phys. Rev. Lett.*, vol. 118, p. 212301, May 2017. [Online]. Available: https://link.aps.org/doi/10.1103/PhysRevLett.118.212301

[10] L. Adamczyk *et al.*, "Measurements of D^0 and D^* Production in $p + p$ Collisions at $\sqrt{s} = 200$ GeV," *Phys. Rev.*, vol. D86, p. 072013, 2012.

[11] A. Adare *et al.*, “Heavy Quark Production in $p + p$ and Energy Loss and Flow of Heavy Quarks in Au+Au Collisions at $\sqrt{s_{NN}} = 200$ GeV,” *Phys. Rev.*, vol. C84, p. 044905, 2011.